March 31st, 2022

Final Report

Research period: July 6th, 2021 to March 31st, 2022

Title:

"Searching the Approaches for Lithium-Ion Battery (LIB) Second Life Performance Improvement"

FRCCP RAS

Daniil Itkis

Summary

Title

Searching the Approaches for Lithium-ion Battery (LIB) Second Life Performance Improvement

Research period

July 6th, 2021 to March 31st, 2022

Delegate of the research

FRCCP Dr. Daniil Itkis

Development / Survey Representative

FRCCP RAS Dr. Daniil Itkis

Conductor

FRCCP RAS Dr. Daniil Itkis

Nissan Motor Co., Ltd. Kazuyuki Shiratori
Yoshiko Hisitani
Takako Toda

Subcontractor/delegate

Purpose

The main aim of the project is to monitor and evaluate promising approaches that can enable enhancement of the LIB performance during its second life (i.e. approaches enabling recovery of battery capacity and/or power after it was used for some time and degraded).

Project Tasks

TASK 1 Cell washing

1.1. Comparison of washing with SCF, subcritical fluid, conventional fluids

1.1.1 HPEC design improvements (conventional fluid compatibility, elimination of side-chain reactions). Fabrication of more HPEC units

1.1.2 Extraction efficiency analysis for single components, whole cells

1.2 SEI/CEI removal analysis

1.2.1 Establishing methodology for SEI/CEI analysis

1.2.2 Analysis of SEI/CEI removal for the electrodes washed by different fluids

1.3 Cell components stability against washing (different ways of washing)

1.3.1 Physicochemical analysis

1.3.2 Electrochemical performance control (linked with 2.2.2)

TASK 2 Cell refiling / recovery

2.1 Auxiliary experiments (pouch cells)

2.1.1 Pouch cell ageing at room temperature

2.1.2 Pouch cell opening/washing/refilling (ordinary electrolyte)/resealing effect on electrochem. Performance

2.2 Recovery using oxidizable Li salts & Li-free oxidizable molecules + LiPF6

2.2.1 Double checking FY20 results on nitrate, lactate in pouch cells

2.2.2 Control experiments on the effect of washing/refilling with the electrolyte in HPEC (linked with 1.3.2)

2.2.3 Model experiments: Artificial Li inventory depletion as a fast ageing tool: testing of the approach.

2.2.4 Testing of recovery electrolyte candidates in HPEC (oxidizable Li salts)

2.2.5 Testing of recovery electrolyte candidates in HPEC (Li-free organic molecules)

2.3 Refiling from donor Li electrode (control)

2.4 Information exchange and results examination with Kansai University

TASK 3 Designing of the cell rigs for commercial cells washing/refilling

3.1. Engineering of the high-pressure reactor with the capability of pouch cell unsealing and resealing

TASK 4 Cell ageing mechanisms in different aging conditions

4.1. Development of the ageing programs

4.1.1. Literature survey on ageing the batteries in EVs

4.1.2. Development of the diagnostic tools to analyze degradation modes of commercial cells

Summary

A new version of HPEC with an O-ring was produced. Corrosion was eliminated. The new HPEC design with a copper pressed current collector was produced. Cycling of the new HPEC is better than for the previous versions but is not good enough yet for the next research actions with HPEC.

A technique for pouch cell washing by supercritical fluids and pure solvents under conditions that are as similar as possible was established. According to the ICP AES data, electrolyte washing efficiency by SC CO_2+MeCN and MeCN at normal pressure is the same for both slightly aged and deeply aged pouch cells. The amount of extracted lithium for deeply aged cells is 2 times smaller.

The SEI layer was studied by TOF SIMS, FTIR, and SEM. It was found that there is no strong difference in the SEI thickness/morphology for different washing procedures (either by SC CO_2+MeCN or MeCN) and both for slightly aged and deeply aged pouch cells.

According to the XRD analysis, the washing procedure does not change the material structure.

A reproducible pouch cell opening/resealing procedure was established and tested. Slightly aged pouch cells that were washed either with SC CO_2 + MeCN or with MeCN and refilled with the ordinary electrolyte show the same capacity that they had before the washing.

Washing of deeply aged pouch cells either with SC CO_2+MeCN or MeCN at normal pressure and their subsequent filling with the ordinary electrolyte (**without** any sacrificial salt added) leads to an **increase** in the discharge capacity of the cells.

Model cells with an additional Li electrode could be aged artificially; in principle, their capacity may be restored using a Li metal donor electrode.

Li_3N is the best sacrificial salt candidate among other oxidizable Li salts and tested organic compounds. Li_3N doesn't dissolve in a $LiPF_6$-based electrolyte.

The use of the Li_3N-based electrolyte could help restore the capacity in either model or pouch cells. But the nitride content in the electrolyte is extremely low, so to yield an actual increase in capacity it is necessary to pump the electrolyte with the sacrificial salt through the cell.

UKansai methods for pouch cell washing and NMC capacity recovery were re-checked. The electrochemical performance of a pouch cell after washing with the electrolyte remains almost the same. The method of NMC recovery leads to an increase in Li concentration in NMC but at the same time the macrostructure of the electrodes was destroyed, they were covered by an insoluble polymer film that prevents cycling of restored electrodes.

Abbreviations

BPR	back-pressure regulator
CV	cyclic voltammetry
DMC	dimethyl carbonate
EC	ethylene carbonate
EIS	electrochemical impedance spectroscopy
HPEC	high-pressure electrochemical cell
ICP AES	inductively coupled plasma atomic emission spectroscopy
LAM	loss of active materials
LFP	lithium iron phosphate $LiFePO_4$
LIB	lithium-ion battery
LLI	loss of lithium inventory
LMO	lithium manganese oxide $LiMn_2O_4$
MeCN	acetonitrile
NMC	lithium-nickel-manganese-cobalt oxide $Li(Ni, Mn, Co)O_2$
PVDF	polyvinylidene difluoride
$scCO_2$	supercritical carbon dioxide
SCF	supercritical fluid
SEI	solid-electrolyte interphase
SEM	scanning electron microscopy
ToF-SIMS	time-of-flight secondary ion mass spectroscopy

Contents

Abbreviations 6

Contents 7

Introduction 9

TASK 1 Cell washing 11

HPEC design improvements 11

Extraction efficiency analysis for single components 14

Comparison of SC CO_2+MeCN and conventional liquids. Optimization of the washing protocol 14

Washing efficiency for cycled cells 17

SEI removal analysis 18

Transfer chamber for ToF-SIMS and SEM measurements 18

Analysis of SEI removal for the electrodes by ToF-SIMS 19

Analysis of SEI/CEI removal for the electrodes by FTIR 21

Analysis of SEI/CEI removal for the electrodes by SEM 23

Analysis of graphite and NMC stability against washing by X-ray diffraction 24

TASK 2 Cell refiling/recovery 26

Auxiliary experiments (pouch cells) 26

Pouch cell ageing at room and elevated temperature 26

Pouch cell opening/washing/refilling (ordinary electrolyte)/resealing effect on electrochemical performance 27

Electrochemical performance of washed/refilled with the ordinary electrolyte aged pouch cell 30

Recovery using oxidizable Li salts & Li-free oxidizable molecules + LiPF6 32

Double checking the CV FY20 together with the Li_3N test 32

Model experiments: Artificial Li inventory depletion as a fast ageing tool: testing of the approach. 35

Refiling from a donor Li electrode (control) 36

Refiling cells by Li_3N electrolyte 37

Reproducing techniques from Kansai University 38

TASK 4 Cell ageing mechanisms in different ageing conditions 41

Literature survey on ageing of batteries in EVs 41

Introduction 41

Principal ageing/degradation mechanisms 42
Ageing mechanisms of battery systems/packs 49
Methods for ageing diagnosis and prognosis 50
Conclusions 53
Outlook 53
References 55

Introduction

The demands for LIBs continue to grow, one of the main drivers today is the production of electric vehicles, which have high energy efficiency (ca. 80% or higher vs. 12-30% for cars with internal combustion engines) [1]. According to various estimates [2,3], the annual amount of LIB waste is *ca*. 200-500 million tons, of which 5-15 wt. % belong to cobalt - an expensive and toxic element, and 2–7 wt.% to lithium. Due to the expected acceleration of LIB production growth, both battery recycling [2–6] and "second life" [7] have become quite hot topics driven by both economic and environmental factors. Although battery recycling is rather cost- and labor-consuming, the increasing amounts of spent batteries push active investments into this field. Reusing spent batteries in the applications not requiring high performance – i.e. battery "second life" – is on the contrary much less expensive. However, there are serious limitations on the energy and power of the spent batteries, so the number of applications is quite limited. The economic benefits of using the spent batteries as is after EoL are also not obvious due to deteriorated performance [7].

This project aims at improving the performance of the spent lithium-ion batteries to enable the use of recovered ones during their "second life" in demanding applications such as electric vehicles. Although recovery of initial properties of as-produced batteries seems to be impossible, we are searching for approaches for partial restoration of battery capacity and/or power. The focus of the project is to evaluate the approach that was suggested at the previous stages to enhance the LIB performance during its second life.

Among numerous reasons for the battery performance loss [8], the group identified as loss of lithium inventory was suggested by us as the most important. In recent years this hypothesis has been confirmed for batteries used in EVs [9] and grid-storage applications [10]. It was also found to be true for various cathode chemistries including NMC, LMO, and LFP. The LLI is driven mainly by damage to the initial SEI layer and its re-formation leading to Li^+ capturing in the form of Li_2O, LiF, Li_2CO_3, and possibly other products. Thus, lithium is partially immobilized in SEI, thus the number of active charge carriers in the cell decreases, and the capacity fades. In addition, excessive SEI increases the negative electrode resistance thus lowering the cell power characteristics.

The main idea for restoring the spent battery capacity is based primarily on removing the old electrolyte and partially the SEI layer from the surface of the negative electrode and further "refilling" of lithium inventory in the cell. This is illustrated in Figure 1, which shows partial immobilization of lithium ions in SEI during battery life, removal of the old SEI, refilling the lithium inventory using special "recovery" electrolytes, and re-formation of SEI (a lithium oxalate additive to prepare the "recovery" electrolyte is shown as an example).

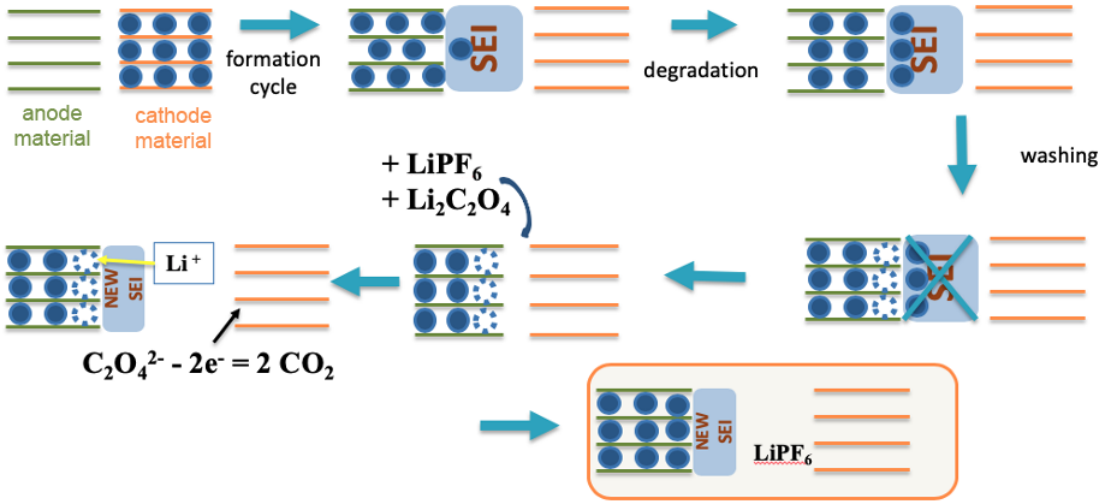

Figure 1. Schematic illustration of the general idea of the project. Lithium host materials are shown as green (anode material) and orange (cathode material) layers. Dark blue circles are lithium ions. Dotted circumflexes denote potential host sites for lithium, which are not filled.

Although complete removal of SEI depicted in Figure 1 has not yet been confirmed, we previously demonstrated the ability to extract the old electrolyte from the electrodes using supercritical fluids together with the SC CO_2+MeCN mixtures, which have good permeation ability (see our previous reports for FY 2018, 2019, 2020). At this project stage, we further investigated the removal of electrolytes from the commercial pouch cells (by SC CO_2 with MeCN as a co-solvent), as well as compared the SC CO_2+MeCN results with the MeCN washing at normal pressure; SEI in the obtained samples was analyzed by ToF-SIMS, FTIR, and SEM. Second, we elaborated and tested the opening/washing/refilling/resealing procedure for the pouch cells. Further on, we performed artificial ageing procedures for a number of cells, tested a new candidate for the recovery electrolyte, Li_3N (in both pouch and “coin-like” cells), and investigated restoration by a metallic Li donor electrode in “coin-like” cells. Finally, we re-checked the results obtained earlier by the Kansai University. The obtained data and their discussion is provided in the report below.

TASK 1 Cell washing

HPEC design improvements

This year we continued to work on improving the HPEC design. The purpose of HPEC development is to perform electrochemical measurements and supercritical extraction experiments without disturbing the separator and the electrodes. In principle, it should be much more reproducible than the pouch cell measurements. HPEC consists of two main parts: the inner 3-electrode electrochemical cell made of PEEK (Figure 2a) and the outer high-pressure cell made of stainless steel (AISI 321). The inner cell ensures a reliable contact between the current collector, the electrodes and the separator (Figure 2b). The outer cell can bear high pressure during the supercritical extraction procedure and contains 5 high-pressure ports: 3 for the electrodes and 2 for supercritical fluid supply.

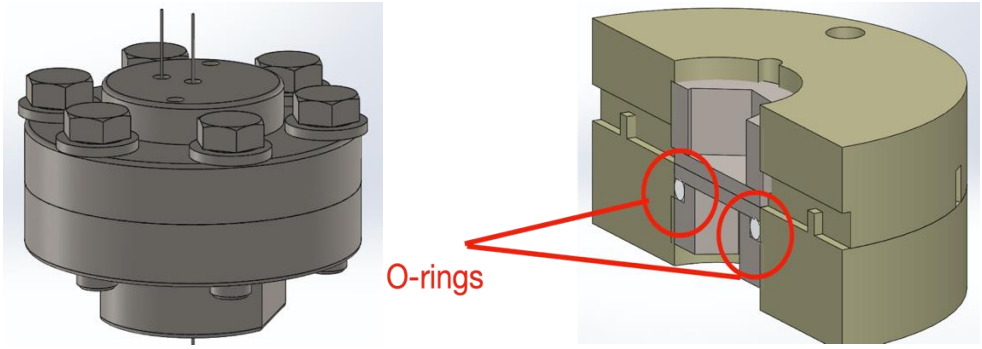

Figure 2. *The outer high-pressure cell body of HPEC made of stainless steel (a) and the inner 3-electrode cell body made of PEEK with o-rings (b)*

At the first step, o-rings were added to the HPEC design (Figure 2b), which were supposed to prevent electrolyte leakage from the cell and the associated corrosion processes, as shown in the figure.

To test the corrosion resistance of this cell, the impedance of the cell with an electrolyte without any active electrode materials was investigated. The results are shown in Figure 3a. It was found that the resistance of the cell does not change significantly over 120 hours, which indirectly confirms the absence of any corrosion processes. However, during the cycling of this cell with NMC and graphite electrodes, it was found that the capacity, even in the first cycle, is significantly lower than the theoretical one and it drops rapidly during cycling (Figure 3b). We associate this process with improper clamping of the electrodes to each other.

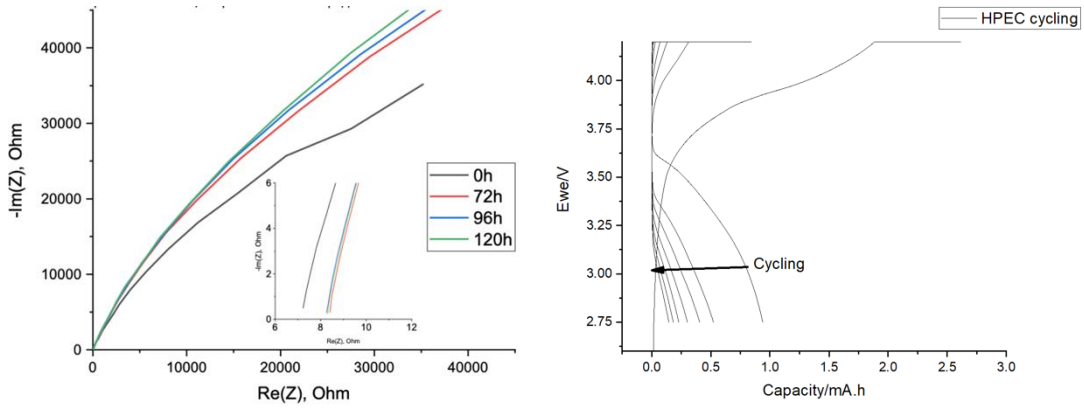

Figure 3. *EIS of the HPEC with o-rings assembled without any active electrode material during 120 hours. (b)Discharge/recharge voltage profiles for HPEC with o-rings assembled with an NMC vs. graphite electrode*

Therefore, at the next stage, a cell with an improved design was developed with more controlled clamping of the electrodes, where a copper plate with a bend was used as a current collector for the negative electrode, which prevents electrolyte leakage (Figure 4).

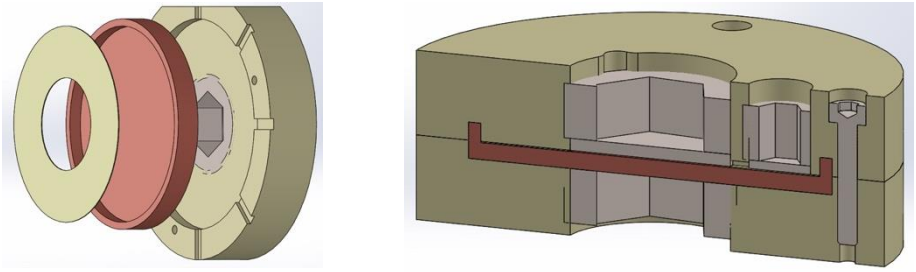

Figure 4. *HPEC with a copper plate with a bend assembly scheme*

The cycling results for this cell with intercalation electrodes are shown in Figure 5. It can be seen that the capacity in the first cycle significantly exceeds that obtained for the previous version of the cell, and the degradation rate also decreased. However, the degradation rate is still high enough for HPEC to conduct precision experiments on the electrode cycling and subsequent washing, therefore the design needs further refinement.

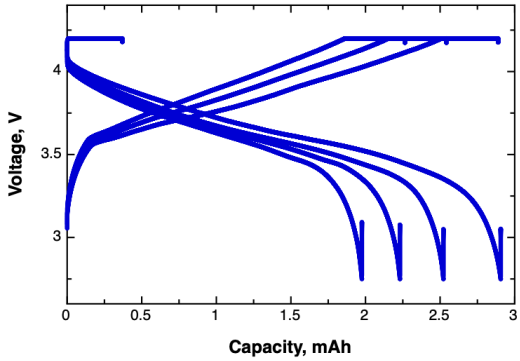

Figure 5. *Discharge/recharge voltage profiles for HPEC with a copper plate with a bend assembled with NMC vs. graphite electrodes*

According to the impedance data shown in Figure 6, this decrease in capacity may be attributed to poor Li transport in the cell. Indeed, the linear region having a 45° slope, which can be associated with distributed Li-ion transport (marked with black arrows in Figure 6) [1], increases by 2 orders of magnitude after a few cycles. This can be either due to electrolyte leakage/evaporation from the system or the formation of some layer with decreased Li conductivity at the electrode surface. Since the refilling of the cell with a fresh electrolyte does not result in any pronounced impedance decrease, the latter appears to be more probable. Further work to detect the layer and distinguish the reason for its formation should be done in the future. Due to the success in developing a reproducible protocol for the pouch cell opening/resealing/refilling, we focused on pouch cell experiments (see below).

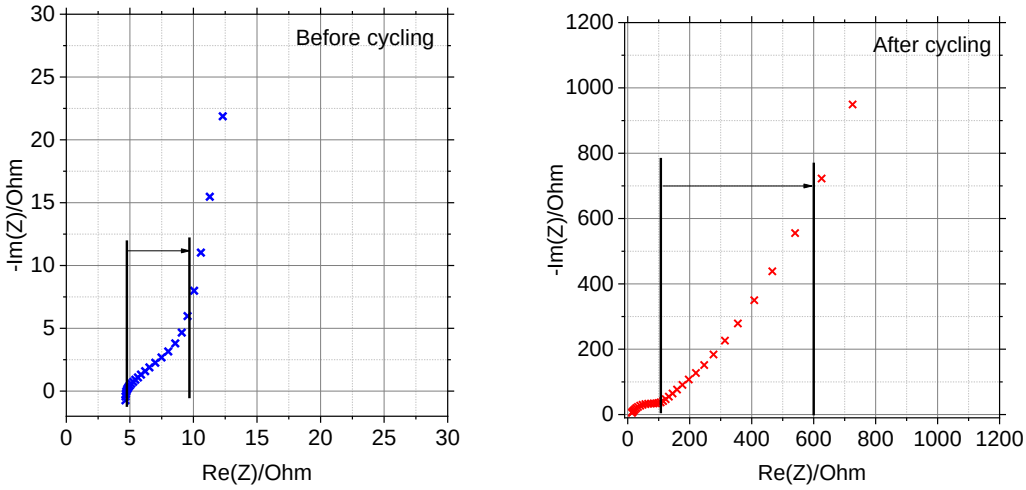

Figure 6*. Nyquist plots of impedance spectra for HPEC with a copper plate with a bend assembled with NMC vs. graphite electrodes before and after cycling. The impedance was measured in a fully discharged state.*

Extraction efficiency analysis for single components

Comparison of SC CO_2+MeCN and conventional liquids. Optimization of the washing protocol

For FY21 the main goal of our project was to compare the washing efficiency of supercritical (SC) fluid and solvents at normal pressure. The experimental details for washing by SC fluid and the co-solvent are given in the FY19/FY20 reports (Figure 7). The CO_2 pressure was set to 300 bar, the thermostat exposition temperature equaled 50 °C, the fluid flow was 4 ml/min. Since we have not achieved reproducible cycling in HPEC up to now, all washing procedures have been performed using pouch cells, for which all the problems with reproducibility have been solved. For the washing procedure, the cells were cut and placed into reactor II, this operation was done inside an argon-filled glove box. The reactor was sealed and isolated by the valves and connected to the high-pressure system. 40 ml of co-solvent (acetonitrile) was poured into reactor I; the entire experimental setup was purged with CO_2 for 90 minutes, and as a result, CO_2 was fed into reactor I, mixed with the co-solvent, got into reactor II, mixed with the electrolyte in the pouch cell and got into the flask with water. Each washing procedure was stopped after washing out 20 ml of the co-solvent.

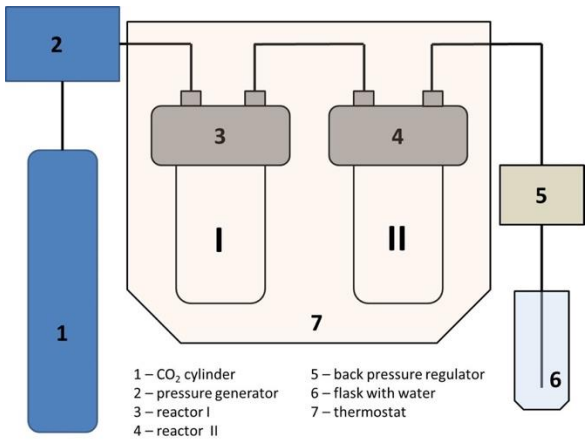

Figure 7. *Supercritical fluid extraction setup scheme.*

Washing in the absence of supercritical fluid was carried out in a setup similar in general to the one shown above. Figure 8 schematically illustrates the washing process. Washing was carried out using an argon flow through a reactor (3) filled with a pure solvent (acetonitrile or dimethyl carbonate). For washing, the cells were cut and placed into the reactor (5), this operation was done inside the argon-filled glove box. The Ar pressure was slightly above 1 bar; V(MeCN) = 20 ml; T = 50 °C.

At the first stage, to search for the optimal technique and compare the washing efficiency, experiments were carried out on pouch cells cycled 10 times (just to test their accuracy).

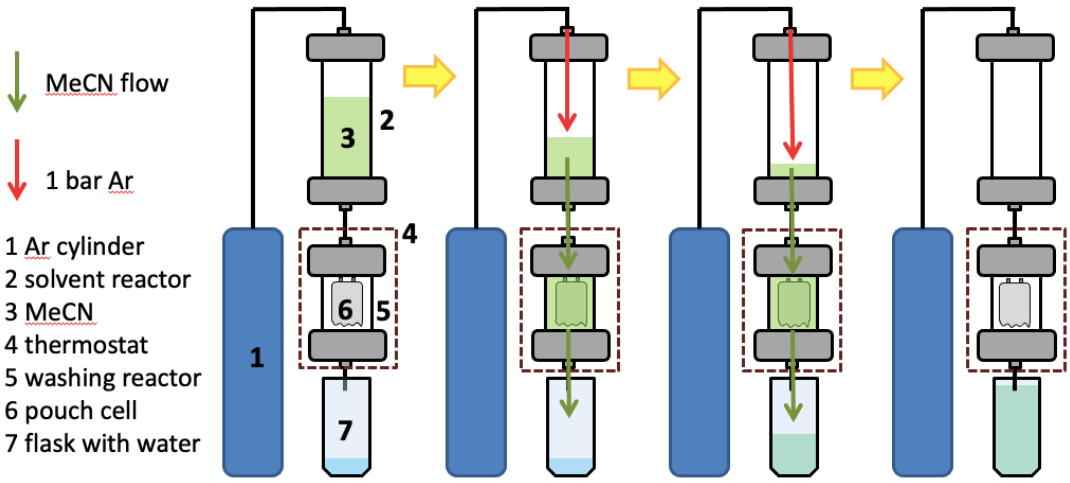

Figure 8. *Normal-pressure solvent extraction setup scheme and the washing process by normal solvents.*

To optimize the washing technique, it was checked how the presence of the shell of the pouch cell, as well as the position of the cut of the shell (when it is not completely removed), affects the efficiency of cell washing by both a mixture of supercritical fluid with MeCN and MeCN at normal pressure. The washing efficiency was monitored by analyzing the lithium concentration in the washing liquid using ICP AES, as well as by analyzing the impedance before and after the washing. The data are shown in Figure 9, as well as in Table 1. Here and below, data on the concentration of lithium are given averaged over at least 3 cells. It was found that the impedance of the cells increases significantly only for washing with a mixture of supercritical fluid and acetonitrile with a completely removed casing. According to the ICP AES data, washing with a fully removed shell in a mixture of acetonitrile with supercritical CO_2 is about 5 times less efficient than with a cut shell. At the same time, the efficiency of washing with acetonitrile at normal pressure does not depend on the shell presence. The lack of resistance change is probably due to the presence of residual acetonitrile, which, when mixed with the residual salt/electrolyte, provides ionic transport within the cell. The Li/P ratio for all experiments does not change within the error and equals 0.8–1, which indicates that the $LiPF_6$ salt is removed during the washing.

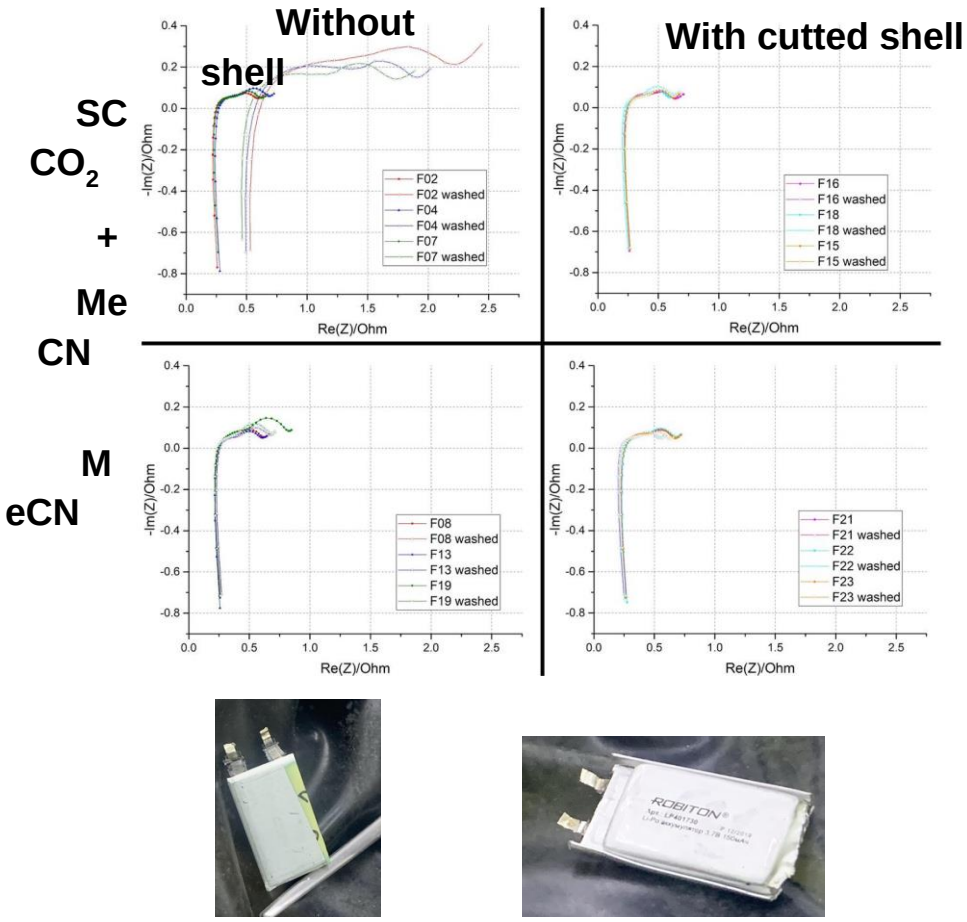

Figure 9. *The EIS spectra of the pouch cells cycled 10 times before and after washing by SC CO_2+MeCN and MeCN at normal pressure with a cut shell and a removed shell. Photo of the pouch cells without the shell and with the cut shell.*

Table 1. *Summarized results of Li and P extraction from ICP AES and resistance from EIS for a cell cycled 10 times by SC CO_2+MeCN and MeCN at normal pressure*

	SC CO_2 + MeCN		**MeCN**	
	Without the shell	Cut shell	Without the shell	Cut shell
Li extracted, µg	950±90	230±90	810±50	830±40
P extracted, µg	5200±700	1100±400	4400±300	4600±300
Li : P, mol:mol	0.8±0.2	0.9±0.1	0.8±0.1	0.8±0.1
Resistance change, %	110±30	4±3	5±4	6±4

Since the amount of Li after washing in acetonitrile at normal pressure (and, therefore, the washing efficiency) is the same with the removed shell and with the cut shell, while handling of cut shell cells is more technologically advanced than the cells with the removed shell, further washing experiments were carried out in a cell with a cut shell.

Further, to optimize the technique, it was analyzed how the position of the cut on the shell relative to the reactor in which the washing was carried out affects the washing efficiency. The ICP AES data for the washing liquid are shown in Figure 10a. It can be seen that the washing efficiency increases significantly when the cut is at the bottom of the cell, both in the case of washing with SC CO_2+MeCN and MeCN at normal pressure. The decrease in the efficiency of flushing when the cell cut is located on top may be due to the fact that the solvent that enters the cell does not leave it and, accordingly, does not enter the collector. Based on the data obtained, all cells were further washed with only one cut located down relative to the reactor.

Also, based on these data, it is possible to compare the efficiency of flushing (the electrolyte removal) with a mixture of SC CO2+MeCN and MeCN at normal pressure. It can be seen that, within the error, the efficiency of washing by these two methods is the same.

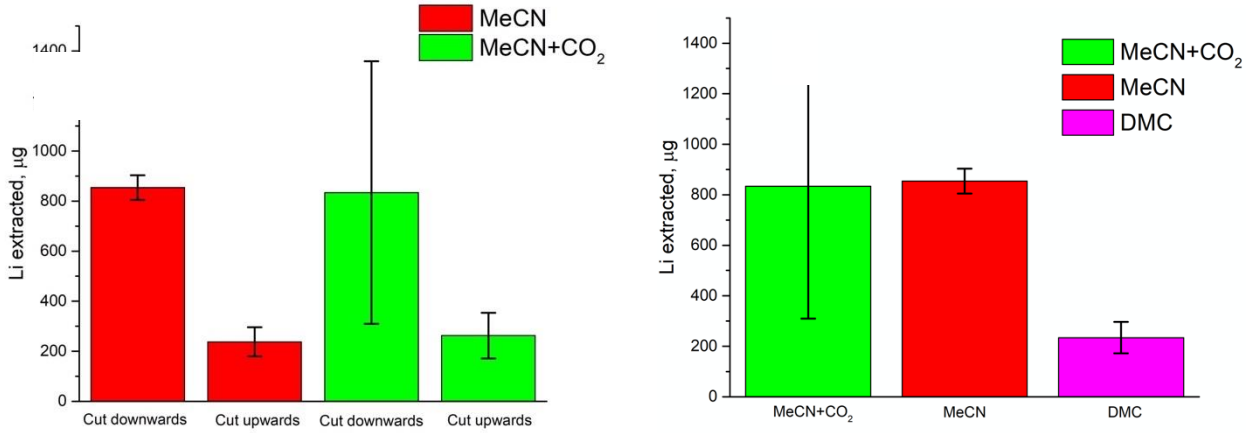

Figure 10. *The amount of lithium measured by ICP AES for cells cycled 10 times, washed by SC CO_2+MecN and MeCN at normal pressure (a) depending on the position of the cut on the shell relative to the reactor, (b) compared to washing with DMC at normal pressure*

As another potential solvent for washing the cell, one of the components of the electrolyte solvent, DMC, was considered. The DMC wash experiment was carried out similarly to the normal pressure MeCN washing. The comparison results for the washing efficiency of DMC with those given above are shown in Figure 10b. It can be seen that the washing efficiency in DMC is about 4 times lower than for SC CO_2 + MeCN and MeCN at normal pressure. This could be attributed to the low polarity of DMC (dielectric constant ε=3.7) compared to acetonitrile (ε=37.5). Therefore, DMC should not be further considered as a cell wash solvent.

Washing efficiency for cycled cells

Figure 11 shows data on the washing of cycled cells with a residual capacity of about 30%. It can be seen that the amount of extracted lithium from cycled cells, as well as from slightly cycled cells, is the same for the mixture of SC CO_2 +MeCN and MeCN at normal pressure, however, the total amount of recovered lithium for the aged cells is 2 times lower (Figure 11a). This observation may indicate that in the case of aged cells, a significant part of lithium passed from the electrolyte to SEI and is no longer available for

washing. The analysis of possible SEI removal by SC CO_2+MeCN and MeCN at normal pressure is given below. Comparing the impedance before and after the washing (an example is shown in Figure 11b), we can say that the impedance decreases slightly when washing the aged cells.

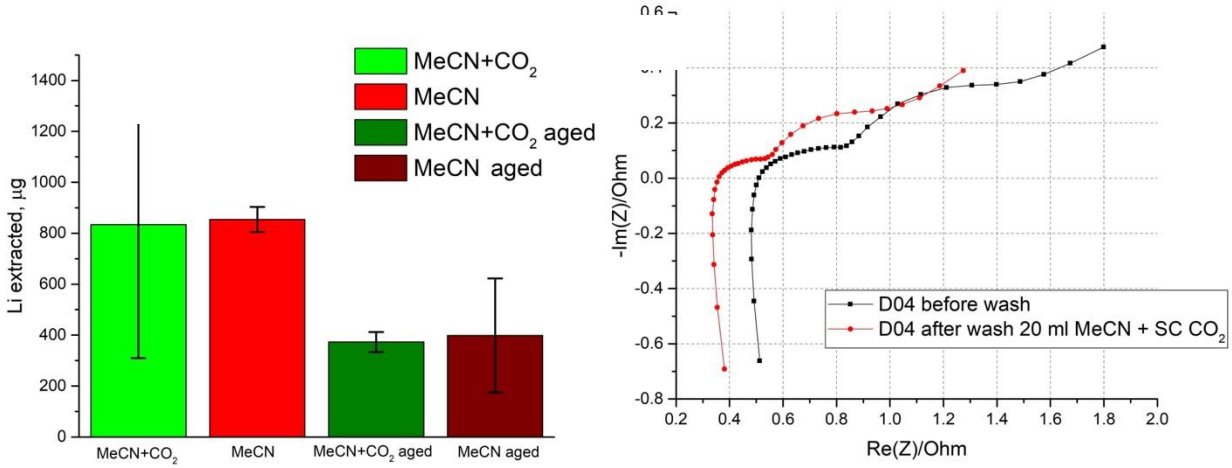

Figure 11. *(a) The amount of lithium washed by SC CO_2+MecN and MeCN at normal pressure for cells cycled 10 times and for aged cells measured by ICP AES. (b) The EIS spectra of an aged pouch cell before and after washing by SC CO_2+MeCN*

SEI removal analysis

Transfer chamber for ToF-SIMS and SEM measurements

To conduct the electrode surface analysis, and, accordingly, to evaluate the efficiency of SEI removal, it is necessary to ensure the transfer of samples from the argon box, where the cell is disassembled, into the analysis chamber of the spectrometer/microscope without any exposure to the atmosphere. To do this, a transfer chamber was made, similar to the one presented in [2], as shown in Figure 12. It can be closed in the argon box by reducing the pressure inside its internal volume. Then, when placed in the spectrometer chamber, it spontaneously opens when the pressure around the transfer chamber drops to a value lower than its internal volume. We used this transfer chamber for SEM and ToF-SIMS analysis of electrode surfaces.

Figure 12. *(a) Closed and (b) opened transfer chamber for SIMS and SEM analysis*

Analysis of SEI removal for the electrodes by ToF-SIMS

The cells after the corresponding ageing/washing procedure were opened in a glove box (<1 ppm H_2O) to remove the anode; all anodes were washed with DMC (for the initial sample, this procedure helped remove the electrolyte, while for other samples after washing it was performed for consistency purposes). All samples were dried under vacuum in the transfer chamber of the glove box. The obtained samples were kept under Ar atmosphere until analysis, thus minimizing exposure to air.

Although the transfer chamber described and illustrated above was used to transfer the samples to the spectrometer, due to the spectrometer configuration, all samples were in the end slightly exposed to air (during several minutes), which, however, does not lead to any significant changes in the SEI/anode profiles based on the available literature data [3]. ToF-SIMS was performed using an ION-TOF-SIMS5 instrument configured with a 30 keV Bi^+ primary liquid metal ion gun at a current density of approx. 1.25 nA/cm^2 in positive ion collection mode with a 150 x 150 μm analysis area. Charge compensation was not used to avoid damage to the delicate SEI layers before data acquisition and the pressure was maintained below $1 \cdot 10^8$ Torr. The mass calibration was performed with reference to the H^+ and Na^+ peaks, and all mass spectra were collected from 1 to 500 amu/z using a reflectron ToF type mass analyzer. Depth profiling was performed first using 1 kV O_2 (which yielded too low etch rate), then using 2 kV O_2 sputtering with a 450 x 450 μm raster area at a current density of approx. 21.8 mA/cm^2 (for 2 kV). No etch rate calibration was performed, therefore the profiles were depicted (and compared) in the “normalized intensity vs sputter time” coordinates. The choice of primary and profiling source was made based on the available literature data.

The obtained ToF-SIMS profiles for positive ions (C^+, Mn^+, Li_2^+) are depicted in Figs. 13-16. Since the electrode consists of individual particles and is not a flat thin film, the ion beam etching/sputtering of the top of the electrode layer does not remove the electrode material uniformly. This causes the SIMS profiles to exhibit broad elemental distributions without any sharp interfaces. Unfortunately, fluorine cannot be analyzed in the available instrument and mode as the method has very low sensitivity for F^+, and its mass is very close to CLi^+ and H_3O^+ ions that can also be present in the SEI. It should be noted that the profile part corresponding to the very beginning of the sputtering process should be disregarded during the profile analysis.

All profiles include similar distinctive features: the C^+ profile has a minimum close to the same sputter time when the Li_2^+ profile has its maximum; the carbon content predictably increases with the profiling time as we are going deeper into the graphitic anode. In our studies, we considered the point corresponding to the Li maximum/C minimum as the SEI boundary. The content of Mn^+ is large in the top part of SEI, then it decreases but there is a second local maximum of Mn in graphite, probably due to its partial intercalation into the anode. Note that we can only draw qualitative conclusions regarding the element depth profiles, and all the graphs in Figs. 13-16 are normalized to the intensity maximum.

The obtained results demonstrate that due to the sample non-uniformity at the microscopic level there is a certain variation of the SEI boundary location even between

two different points on the same sample (350 s vs ≈400 s sputter time in Fig. 13, i.e., up to 50 s scattering between different sample points). Fig. 14 shows the profiling results for the slightly aged cell as it is, after its washing with MeCN and with SC CO_2 + MeCN. The obtained profiles are similar, and the SEI boundary location drawn as described above is the same for all three samples under consideration, therefore, the washing procedure does not seriously affect the SEI thickness and composition. For the significantly aged cells (Figs. 15-16), virtually no Mn+ was observed during profiles, which is quite an odd result that can be explained by either deeper Mn intercalation into the graphitic anode, or alternatively by its deintercalation and removal from the SEI layer during cycling compared to the initial slightly aged cells. For this reason, the SEI boundary location was determined based on the Li_2^+ maximum only for the significantly aged samples. As shown in Fig. 15, due to thicker SEI the 1 kV O_2 sputtering leads to even broader profiles with very indistinct maxima, which illustrates why 2 kV O_2 sputtering was used in our experiments for significantly aged cells (which increases the sputtering rate by almost 4 times, so graphs in Figs. 13-14 and Figs. 15-16 are not directly comparable, the 4x factor should be taken into account). Both lithium and carbon profiles have the same features as for the slightly aged cells in Figs. 13-14. Interestingly, for the significantly aged cells washing with MeCN significantly (2x) increases the observed SEI thickness, while washing with SC CO_2 + MeCN does not lead to any significant SEI thickness variation compared to the unwashed cell anode; the Li profile in the case of MeCN washing becomes broader, which may also suggest changes in the SEI thickness. In all cases, the SEI thickness is notably higher than for the slightly aged cells. Additional experiments involving both detailed analysis of the ions obtained in ToF-SIMS and negative ion depth distribution should be performed to get further insight into the reasons for the SEI thickness difference as well as the related mechanisms.

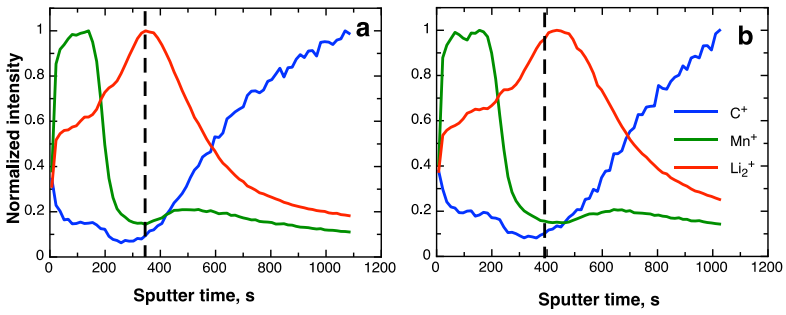

Figure 13. ToF-SIMS profiles of a slightly aged cell anodes before washing:different points on the same sample (the profiles were obtained with 1 kV O_2)

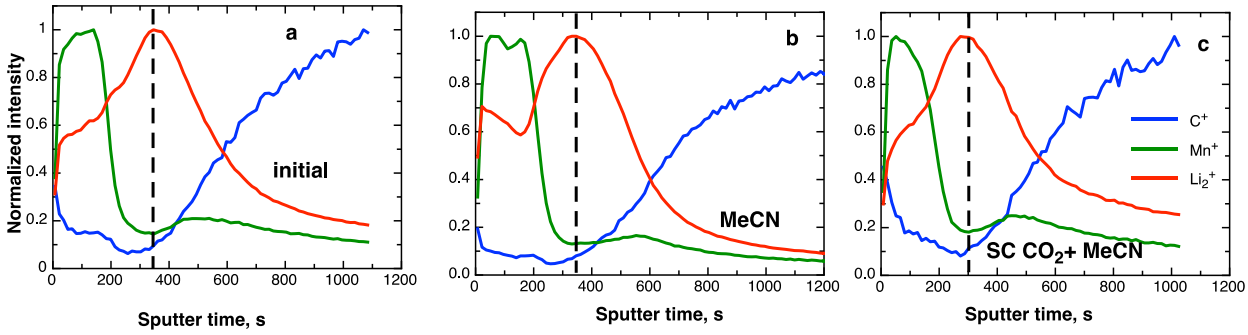

Figure 14. ToF-SIMS profiles of slightly aged cell anodes: (a) an initial (non-washed) cell, (b) a similar cell washed with MeCN, (c) a similar cell washed with SC CO_2 + MeCN (all data was taken during 1 kV O_2 sputtering

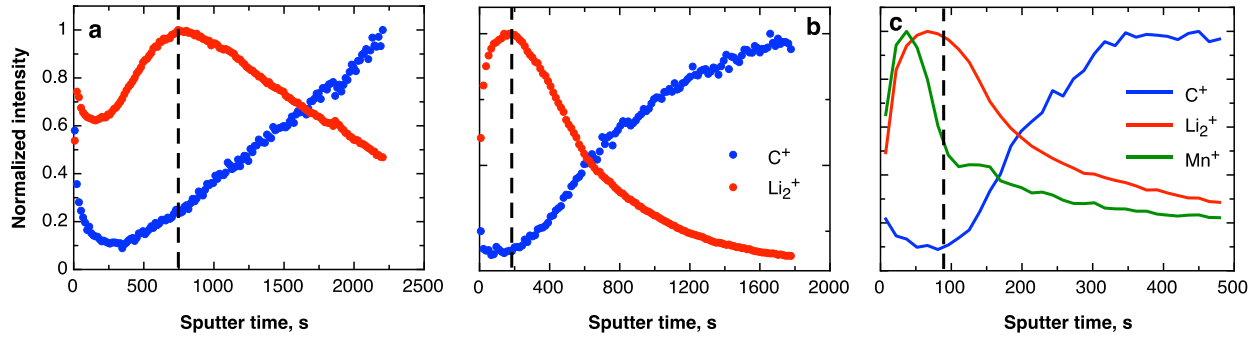

Figure 15. ToF-SIMS profiles of significantly aged cell anodes before washing: (a) obtained with 1κV O_2 sputtering; (b) obtained with 2 kV O_2 sputtering; (c) obtained with 2 kV O_2 for a slightly aged for comparison.

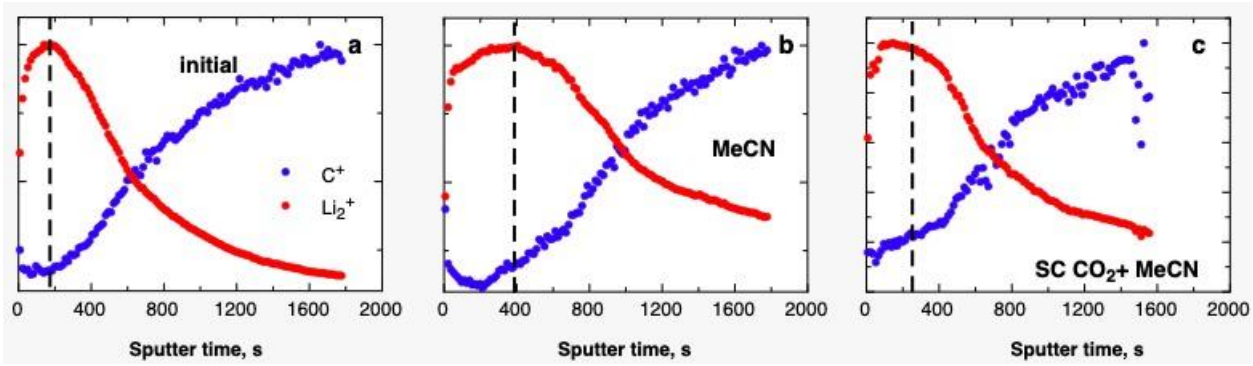

Figure 16. ToF-SIMS profiles of significantly aged cell anodes: (a) an initial (non-washed) cell, (b) a similar cell washed with MeCN, (c) a similar cell washed with SC CO_2 + MeCN (all data was taken at 2 kV O_2 sputtering

Analysis of SEI/CEI removal for the electrodes by FTIR

The electrodes were also analyzed using FTIR on a Bruker Alpha II spectrometer in an argon box to carry out the analysis without exposure to the atmosphere. Sample preparation was performed similarly to the study by the ToF-SIMS method, but drying in vacuum was not performed.

Figure 17 shows the spectra of electrodes from a cell cycled 10 times. The spectra of both cathodes and anodes do not differ significantly before and after washing by various methods. A list of assigned peaks is given in Table 2. It can be seen that both graphite peaks and the peaks characteristic for SEI are present at the anode surface. In the spectrum of the cathode, the most intense signals correspond to graphite (apparently, a carbon additive to the electrode material), as well as to the signal from NMC. It should be noted that the depth of analysis by the FTIR ATR method is 1–2 μm, which does not provide sufficient surface sensitivity for the SEI analysis, and this method can be considered rather as an additional method to simplify the interpretation of methods with higher surface sensitivity, such as ToF-SIMS.

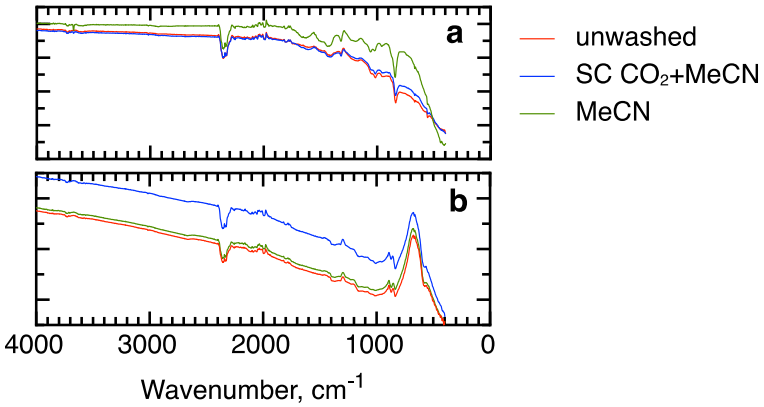

Figure 17. *FTIR spectra of an anode (a) and a cathode (b) from an unwashed aged pouch cell and a similar cell washed by different methods*

Table 2. *Assignment of selected vibrational modes*

Wavenumber, cm^{-1}	Assignment	Reference
2353, 2327	Graphite	[4]
823, 1309	$ROCO_2Li$	[5,6]
1003	DEC C–C–O asymmetric stretch	[4]
542	LiPF6	[4]
670	MO6 groups	[7]

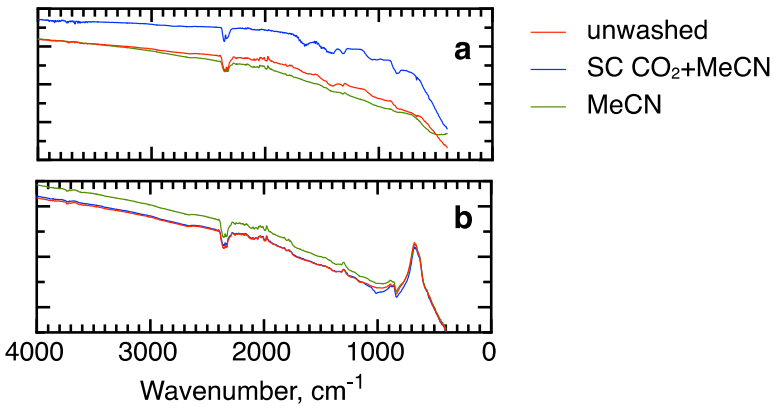

Figure **18** shows the surface spectra of cathodes and anodes from aged cells, both unwashed and washed by various methods. Comparing these spectra with the spectra of the slightly cycled cells, it can be seen that the most intense peaks corresponding to graphite and MO_6 bond vibrations are preserved, while the weaker signals corresponding to the organic component decrease, which contradicts the notion that aged cells have a greater SEI/CEI thickness. The decrease in signal intensity may be due to the absorption of infrared radiation by the SEI/CEI layer.

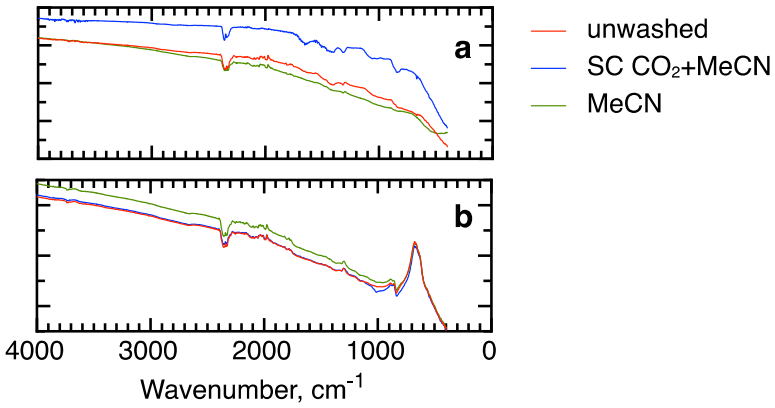

Figure 18. *FTIR spectra of an anode (a) and a cathode (b) from an unwashed aged pouch cell and a similar cell washed by different methods*

Analysis of SEI/CEI removal for the electrodes by SEM

A field-emission SEM (Carl Zeiss Supra 40) was used for the graphite electrodes morphology studies for aged cells without washing as well as for similar cells washed with a supercritical fluid with acetonitrile or pure acetonitrile at normal pressure. Sample preparation was performed as described above for ToF-SIMS, and transfer of samples to the microscope without contact with the atmosphere was carried out using the transfer chamber. The results are shown in Figure 19.

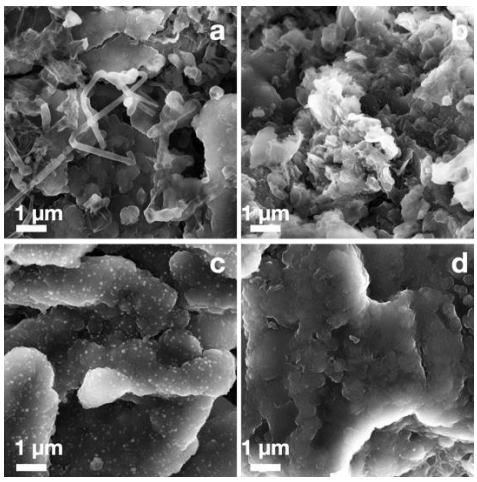

Figure 19. *SEM images of a graphite electrode surface of aged cells (a,b) without washing (c) washed by SC CO2+MeCN (d) MeCN at normal pressure.*

Spheres, threads on the surface of an unwashed graphite electrode are observed in Figure 19a. In general, the entire surface consists of fused hemispheres. Such a picture (the presence of spherical formations) is typical of the SEI morphology on graphite. Since we do not have the technical ability to analyze the surface of the original electrode before cycling, the micrograph of the area in Figure 19b, which was obtained as a result of mechanical damage to the electrode surface, indirectly illustrates the initial graphite morphology: individual graphite flakes not covered with a film. In the micrographs of electrodes from the washed cells (Figure 19c,d) one can also notice the presence of fused hemispheres that is typical for the SEI morphology on graphite [8,9], however, large individual spheres or threads are not observed on the electrode surface, which may indirectly indicate partial removal of SEI from the electrode surface. In this case, the absence of graphite flakes on the electrode surface unambiguously indicates that the complete removal of SEI does not occur, which is consistent with the ToF-SIMS data.

Analysis of graphite and NMC stability against washing by X-ray diffraction

Additional physicochemical analysis of electrodes from either washed or unwashed aged cells was carried out by X-ray diffraction (XRD).

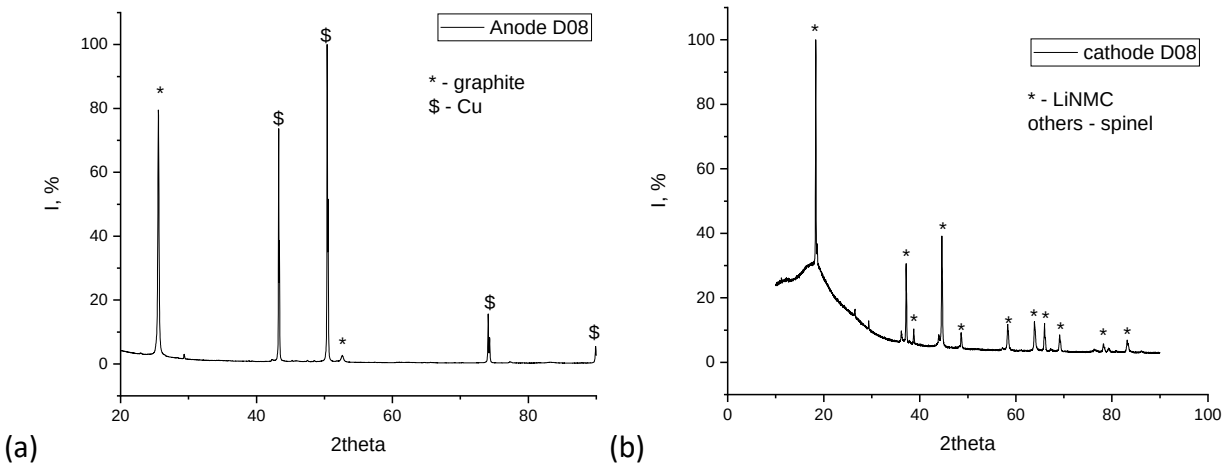

Figure 20. *XRD patterns of graphite (a) and NMC (b) electrodes of the aged cells washed by SC CO_2+MeCN*

For the anodes, the XRD pattern features copper and graphite reflections. Unfortunately, only *00l* peaks are visible for graphite, so just the *c*-parameter could be refined correctly. Table 3 provides the values for the (002) d-spacing (i.e. the distance between the graphene layers in the material).

Table 3. *d-spacing for the graphite species.*

Material	D-spacing, Å	x in Li_xC_6 [10]
B-Graphite	3.347 [10]	0
Unwashed anode	3.438	0.14
SC CO_2+MeCN washed anode	3.478	0.26
MeCN washed anode	3.496	0.32

For the cycled anodes, the d-spacing is similar to Li_xC_6 for x=0.14-0.32. However, for similar uncycled anodes (both washed and unwashed)the d-spacing does not exceed 3.37 Å, and for Li_xC_6 x<0.02. While for uncycled anodes the d-spacing dispersion is quite small, the difference between washed and unwashed cycled anodes can be caused by different fading states of different batteries in analysis.

For the cycled cathodes, the XRD pattern consists of NMC, spinel (an NMC decomposition product), and minor Al peaks. The NMC lattice parameters are given in Table 4.

Table 4 Lattice parameters for NMC, s.g. R-3m

Material	*a*, Å	*c*, Å
Unwashed anode	2.8355	14.4351

SC CO_2+MeCN washed anode	2.8292	14.4743
MeCN washed anode	2.8310	14.4657

All cell parameters are quite similar for all cathodes, and compared with uncycled cathodes the *a* parameter is lower (avg. 2.855 Å), while *c* is higher (avg. 14.33 Å). This is typical for NMC electrodes and has been described in the literature [11]. This is associated with LLI, however, precise calculations are impossible as the initial NMC composition is unknown.

TASK 2 Cell refiling/recovery

Auxiliary experiments (pouch cells)

Pouch cell ageing at room and elevated temperature

The pouch cells for cycling and washing experiments were similar to those used last year. The used cells were produced by EEMB ltd. (model LP401730). Detailed characteristics are presented in the FY20 report. This year, for the first time, their long-term cycling for 500 cycles or more was carried out for about 3 months. The cycling parameters are also similar to those used in the previous year: rate c/2, potential range 2.75-4.2V. Figure 21 shows the capacity fade during cycling for two experimental series. Figure 21a illustrates that after approximately 500 cycles, the capacity fade rate increases significantly and by the 700th cycle it is about 30% of the initial value. Since the goal of this study is to clarify the possibility of restoring cells with a residual capacity of about 80%, another series of cycling experiments was carried out, as shown in Figure 21b. The average remaining capacity for this series as of February 9, 2022 is 87%, however, there are several cells for which capacity has already reached the target value of 80% and the number of such cells increases over time.

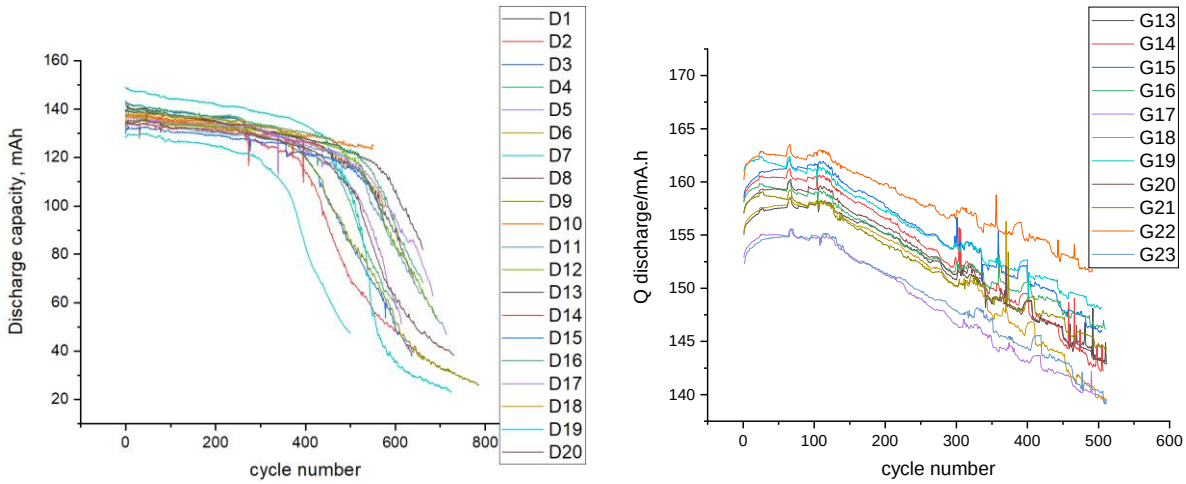

Figure 21. *Capacity fade for the pouch cells during cycling for 2 experimental series*

To increase the cell degradation rate, we performed cycling at an elevated temperature (T=50^0 C). The results are shown in Figure 22. Under such conditions, the rate of capacitance decline increases, and with a similar number of cycles (500), the capacitance reaches 78% (Figure 22a). A comparison of the discharge-charge curves at the 300^{th} cycle is shown in Figure 22b. It can be seen that the charge voltage for a cell cycled at an elevated temperature is higher than for a cell cycled at room temperature, while the voltage is lower. However, these differences are more likely due to the fact that they have different capacities at the 300^{th} cycle, as the general course of these curves coincides.

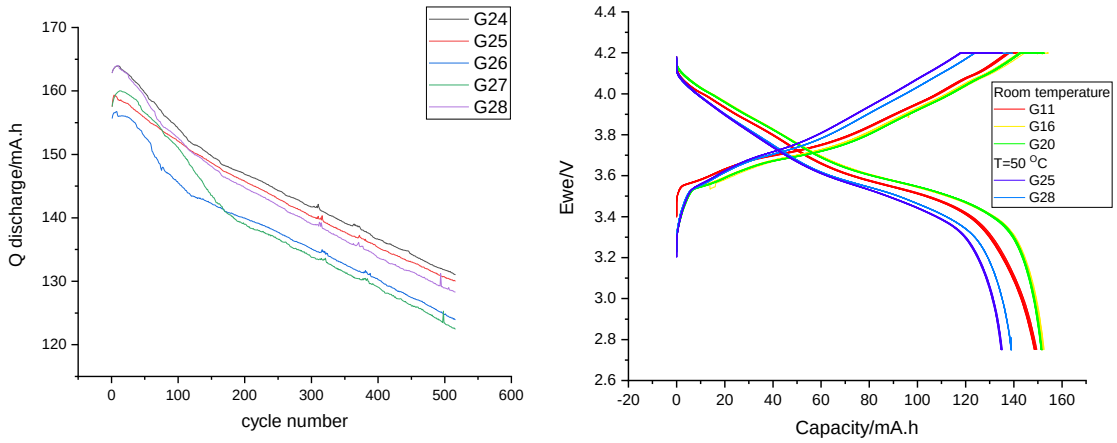

Figure 22. *(a) Capacity fade for cells cycled at 50^0 C.(b) Discharge/recharge voltage profiles at the 300th cycle for cells cycled at RT and at 50^0 C.*

Pouch cell opening/washing/refilling (ordinary electrolyte)/resealing effect on electrochemical performance

To perform a precise study of the effect of washing and refilling with an electrolyte on the pouch cell capacity, it is necessary to be sure that the cutting and sealing of the cells do not affect their performance. This year, we carried out methodological work on the selection of optimal conditions for cutting with control of the discharge capacity after refilling them with the electrolyte and sealing. This technique was tested on cells before manipulations for 10 cycles to control their performance. Figure 23 illustrates the cell opening methods that we are considering. 1. Cut from the bottom side (Linecut). 2. 2 cuts on one side of the shell, with the removal of a quarter of the cell shell (Halfcut). 3. 4 cuts on one side of the body and removal of half of the cell shell (Fullcut).

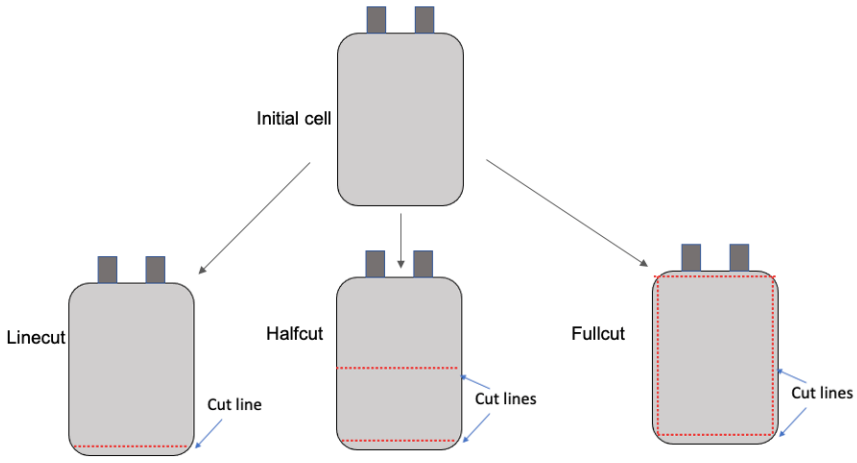

Figure 23. Illustration of the cell opening methods employed

The sealing methods corresponding to the given cutting methods are shown in Figure 24. Before sealing, 60 µl of 1M LiPF6 EC:DMC electrolyte (Aldrich) was added to the cell. Cells were sealed using a special Teflon tape manufactured by MTI, the adhesive layer of which is resistant to interaction with the electrolyte. Cycling was carried out in a

sealed container to exclude the influence of moisture and atmospheric oxygen on the cycling process.

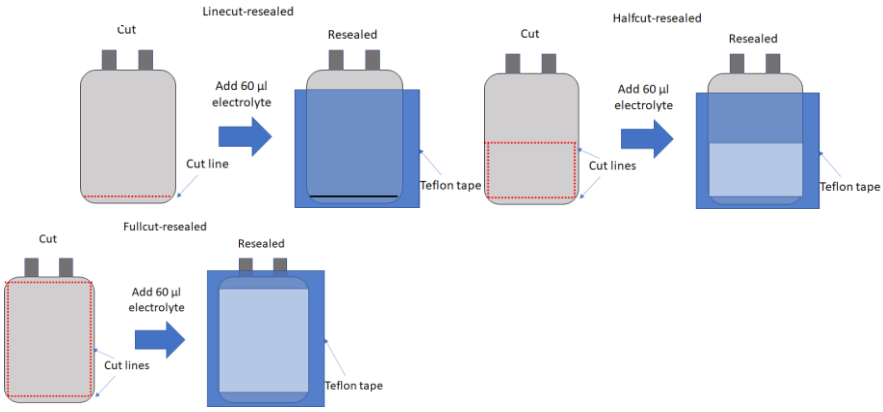

Figure 24. *Resealing procedure after various opening methods (a) Linecut, (b) Halfcut, (c) Fullcut*

The results of cycling for the cells opened and sealed by each of the methods are shown in Figure 25Figure **27**. In the case of opening with 4 cuts, the cell capacity is immediately reduced by 1.6 times (from 130 to 80 mAh) (Figure 25), therefore this opening/sealing method is not suitable for use. When opened with two cuts, after refilling the cell with electrolyte and sealing, the discharge capacity coincided with the capacity before filling with the electrolyte (Figure 26). The behavior of the discharge curves did not change. However, the capacity fade rate increased significantly compared to that before the manipulations (Figure 26b). Therefore, this method of cutting is also not optimal. Finally, opening cells with one cut at the bottom (Linecut), with subsequent sealing, does not lead to any significant capacity change (it even slightly increases, which may be due to the higher ionic conductivity of the electrolyte we use, as well as more efficient compression of the electrodes), nor to a change degradation rate (Figure 27). Therefore, for further experiments to control the effect of cell washing/refilling on the electrochemical performance, the linecut method was used.

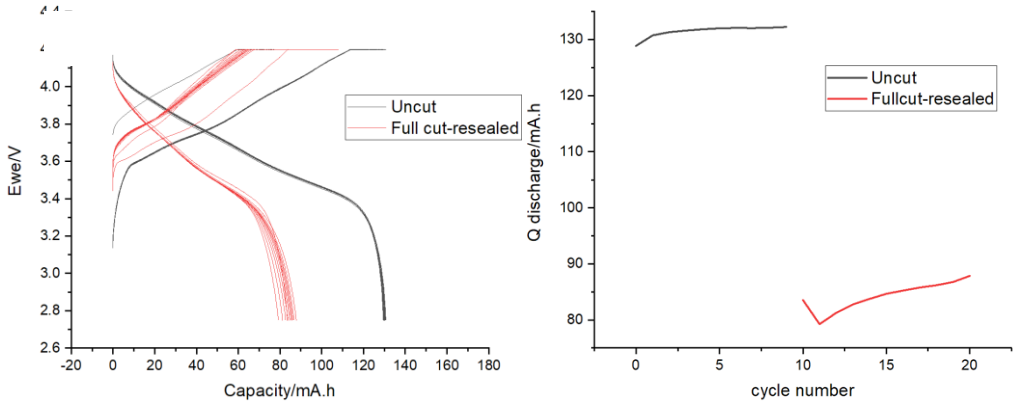

Figure 25. *Discharge/recharge voltage profiles (a) and capacity fade (b) for a cell before cut and after a Fullcut open/reseal procedure*

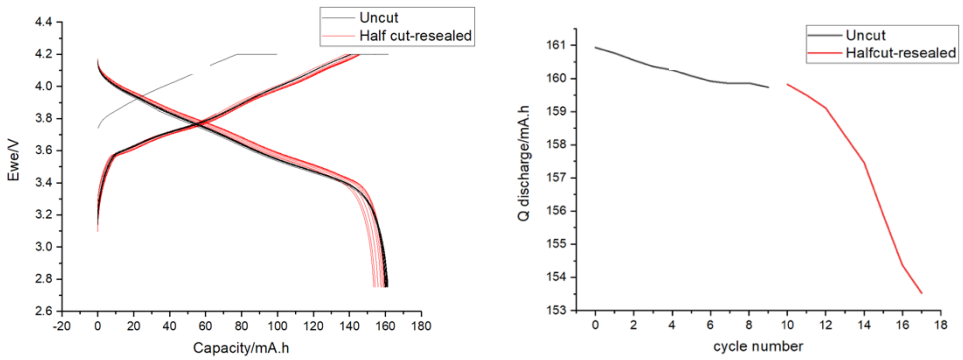

Figure 26. *Discharge/recharge voltage profiles (a) and capacity fade (b) for a cell before cut and after a Halfcut open/reseal procedure.*

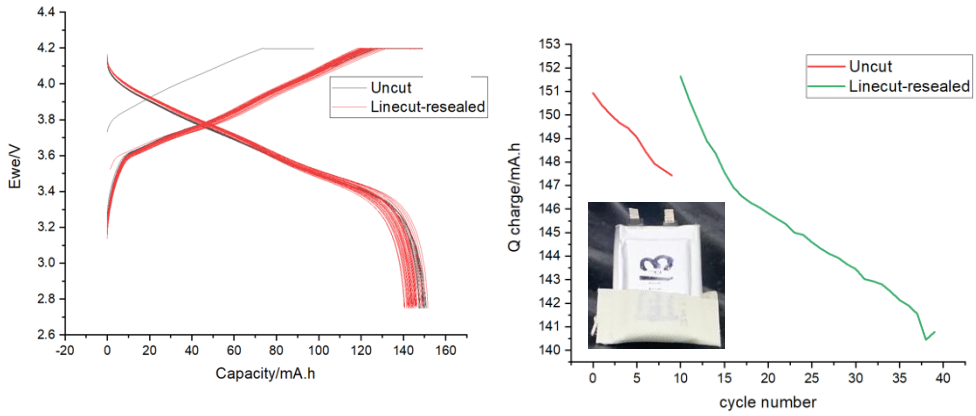

Figure 27. *Discharge/recharge voltage profiles (a) and capacity fade (b) for a cell before cut and after a Linecut open/reseal procedure. Insert in (b): photo of a Linecut resealed pouch cell.*

The effect of washing by both SC CO_2+MeCN and MeCN at normal pressure on the electrochemical performance of the pouch cells, as well as in the previous case, at the first stage, was investigated for cells cycled 10 times. The results are shown in Figure 28Figure **29** (for each washing method 2 experiments were carried out with similar results). During this experiment, the cells were opened by the Linecut method, then washed with either SC CO_2+MeCN or MecN, filled with 200 µl of 1M LiPF6 EC:DMC electrolyte (Aldrich), and finally cycled in a sealed container. It can be seen that in both cases, an increase in the discharge capacity by several mAh is observed, similar to what was observed in the case of adding an electrolyte to an unwashed cell. The shape of the discharge curve remains unchanged, the degradation rate increases, but not very significantly. Therefore, it can be concluded that washing with both SC CO_2+MeCN and MeCN at normal pressure, followed by filling with the ordinary electrolyte and sealing of the cell, does not significantly affect the electrochemical characteristics of the pouch cell. Accordingly, this method of processing pouch cells can be used to study the effect of washing and refilling for aged cells.

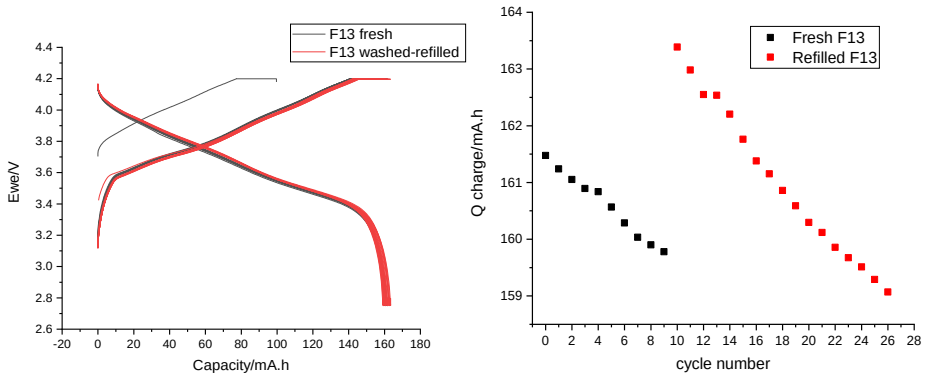

Figure 28. *Discharge/recharge voltage profiles (a) and capacity fade (b) for a cell cycled 10 times washed by SC CO_2+MeCN*

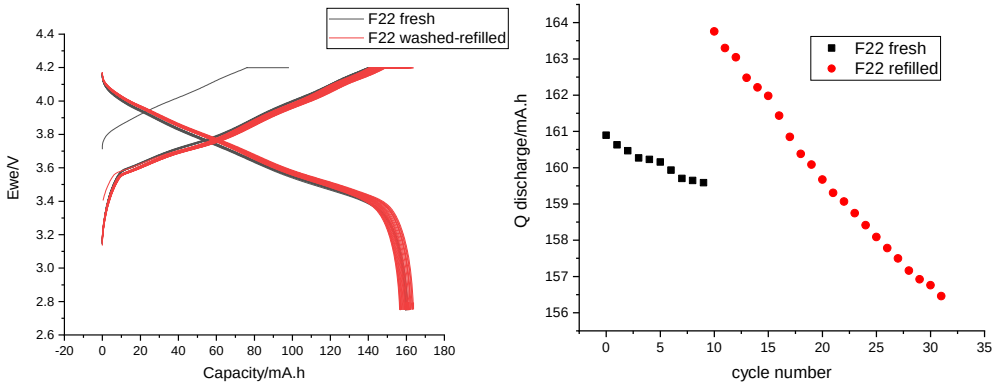

Figure 29. *Discharge/recharge voltage profiles (a) and capacity fade (b) for a cell cycled 10 times washed by MeCN at normal pressure*

Electrochemical performance of washed/refilled with the ordinary electrolyte aged pouch cell

The most interesting results were obtained regarding the electrochemical performance of aged cells after their washing and refilling with the electrolyte. This experiment was carried out in the same way as shown above. Figure 30 shows the capacity data after washing and refilling with the electrolyte, the remaining capacity is about 30% of the original value. In the case of washing with MeCN at normal pressure, the capacity after refilling with electrolyte increases by almost 2 times and by more than 1.5 times after flushing with a mixture of supercritical fluid with acetonitrile. At the same time, in the case of opening and adding the electrolyte without the washing procedure (blue curve), the capacity decreases. As of February 21, a total of 6 refilling experiments has been carried out, and the corresponding data are collected in Table 5. From the data obtained, it can be concluded that washing either by SC CO2+MeCN or MeCN at normal pressure and filling with the ordinary electrolyte (1M LiPF6 EC:DMC) **without** any sacrificial salt leads to an **increase** in the discharge capacity of the cells.

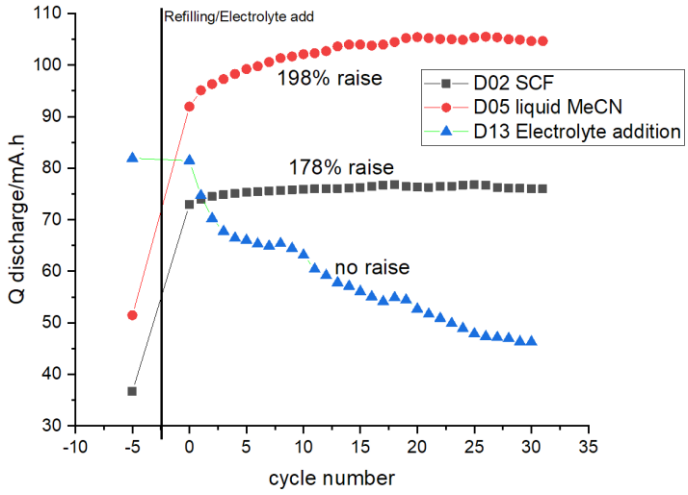

Figure 30. *Capacity vs. cycle number for an aged pouch cell unwashed and washed by different methods and refilled with the ordinary electrolyte*

Table 5. *Change of capacity of an aged cell after washing and refilling with the ordinary electrolyte*

Washing method	Capacity before washing, mAh	Capacity after washing, mAh	Increase of capacity (%)
SC CO_2+MeCN	36	73	203
	57	89	156
MeCN at normal pressure	51	92	180
	23	50	217
No washing, electrolyte added	82	81	0
	94	106	112

We also conducted an additional experiment to study the washing efficiency, and one cell washed initially with SC CO2+MeCN was washed again after the primary washing to investigate the possible removal of the aged electrolyte/SEI not removed at the first stage. The capacity data is shown in Figure 31. It can be seen that if after the first washing the capacity changed by 200%, which was noted earlier, then after the second washing the capacity increased by just 4%. Therefore, during one washing cycle, it is

possible to extract all substances available for removal by this method, which are responsible for the capacity fade of the pouch cell.

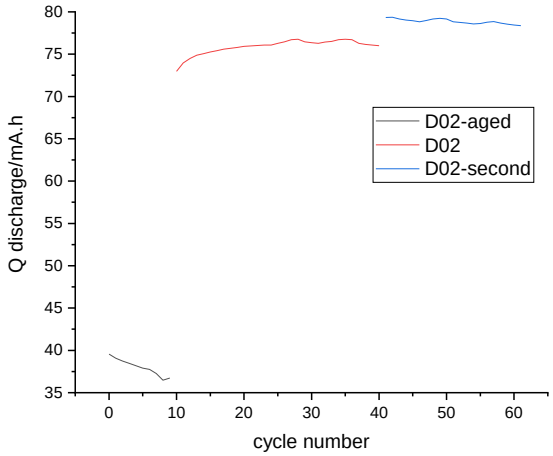

Figure 31. *Capacity vs. cycle number for an aged pouch cell that was washed by SC CO_2+MeCN 2 times*

Recovery using oxidizable Li salts & Li-free oxidizable molecules + LiPF6

Repeated SEI formation leads to active lithium inventory loss, thus, the stated red/ox balance between the cathode and the anode materials becomes disrupted (see Figure 1). To balance the red/ox processes and recover the lithium inventory, we tried several additions to the electrolyte as shown in Figure 32. While selecting additives for the tests, we used two criteria: 1) the additive hypothetically can be oxidized irreversibly at moderate potentials with gaseous products formation; 2) it should be stable to reduction at moderate potentials.

Double checking the CV FY20 together with the Li_3N test

Most of the salts analyzed this year were similar to those tested in the past, but this year the experiment was done more precisely. A 3-electrode glass electrochemical cell shown in Figure 32 was used. 1M $LiClO_4$ in EC:DMC was used as the base electrolyte. Solutions with poorly soluble salts (lactate, acetate, nitride) were prepared by mixing an excess of a solid salt with a base electrolyte for 5 days with a magnetic stirrer, then filtering through a syringe filter. Solutions of nitrate, methyl formate, and dimethyl oxalate were prepared at the concentrations shown in Figure 32. A GC electrode (ALS Co., Ltd.) was polished by 0.06 μm silica and ultrasonicated in water before the experiment. A platinum wire was used as a counter electrode. An Ag^+/Ag Vycor frit separated electrode with 0.01 M $AgNO_3$ (ultrapure, Reakhim) and 0.1 M tetrabutylammonium perchlorate ($TBAClO_4$, for electrochemical analysis, ≥99.0%, Sigma-Aldrich) in MeCN was employed as a reference electrode. The reference electrode potential was calibrated versus the ferrocenium/ferrocene couple (98%, Aldrich). The measurements were carried out in an argon box to minimize the possible effect of moisture and oxygen on the experimental conditions.

The voltammograms at 100 mV/s are shown in Figure 32. The black voltammogram is for the base electrolyte. It can be seen that it is electrochemically stable in the studied potential range. At the same time, when any of the considered additives is added, an increase in the anode current is observed at potentials above 5 V, which indicates that oxidizing additives are present in the electrolyte. Nitrate and nitride demonstrate the highest values of the anode current; however, in the case of lithium nitrate, its recovery is also observed at a potential below 3 V. Therefore, this electrolyte cannot be considered as a potential candidate for sacrificial salt.

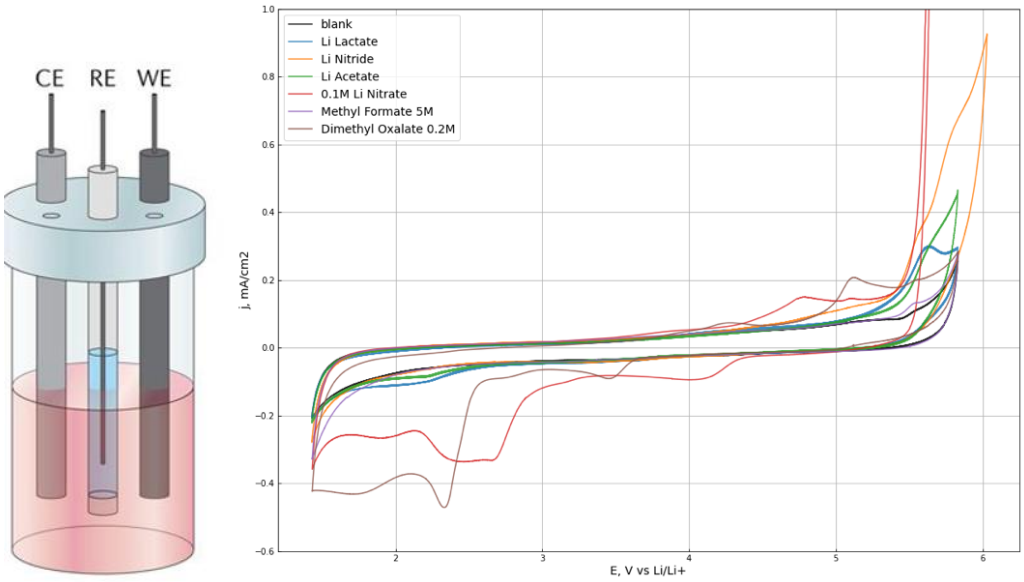

Figure 32. *Scheme of the three-electrode electroanalytical cell (left) and CV curves (right) for the tested candidates for the recovery electrolyte.*

A photograph of a saturated solution of lithium nitride is shown in Figure 33a. The Li_3N solution has acquired a yellow tint. To track the Li_3N solubility mechanism and the presence of possible side reactions, we registered the FTIR spectra of the initial electrolyte and the saturated solution (Figure 33b). There are no significant changes in the spectra, so lithium nitride is soluble in EC:DMC in the absence of any side reactions. It should be noted that, according to the literature data, lithium nitride has low solubility in lithium-containing electrolytes and high reactivity with respect to a number of widely used solvents, such as acetonitrile, since it is a strong nucleophile.

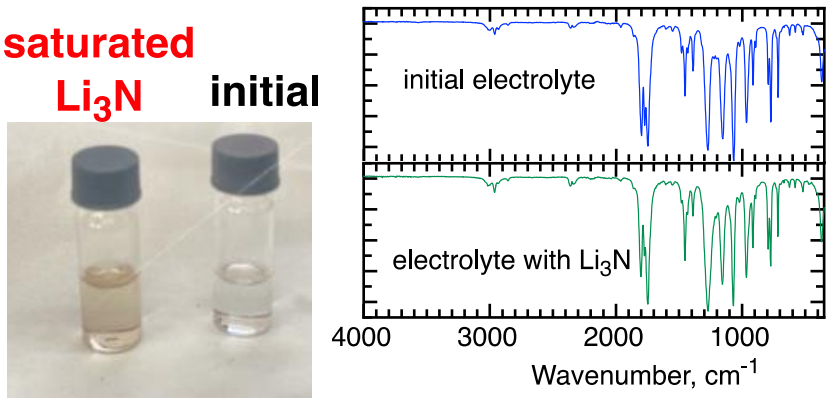

Figure 33. *Photo (a) and FTIR spectra (b) of the initial electrolyte and the electrolyte saturated with Li_3N*

Therefore, lithium nitride is the most promising candidate as a sacrificial salt among the tested compounds.

The above experiments were carried out in a solution of 1M $LiClO_4$ in EC:DMC. However, the electrolytes of commercial lithium-ion cells are $LiPF_6$-based. Therefore, we further performed a similar experiment on the dissolution of Li_3N in 1M $LiPF_6$ in EC:DMC. Voltammograms of a pure electrolyte solution and a solution after exposure to solid lithium nitride are shown in Figure 34. It can be seen that the current density in the nitride solution is even lower than in the blank electrolyte. From this, it can be concluded that Li_3N does not dissolve in the $LiPF_6$-based electrolyte, which is possibly due to the chemical interaction of Li_3N with traces of HF in the electrolyte, which led to the passivation of the surface of the lithium nitride powder by the LiF layer and therefore prevented the dissolution of Li_3N.

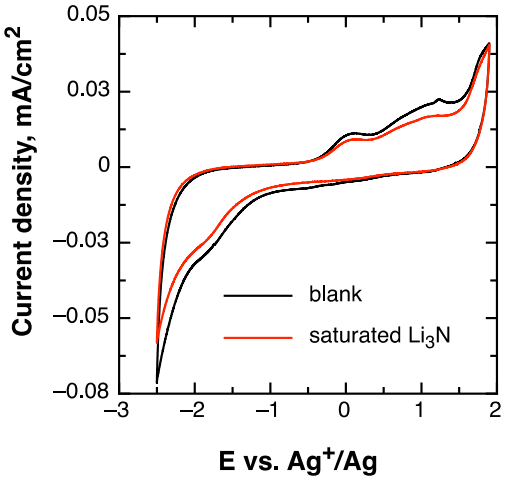

Figure 34. *Voltammograms of a GC electrode in 1M $LiPF_6$ in EC:DMC and a saturated solution of Li_3N in 1M $LiPF_6$ in EC:DMC*

Therefore, further a saturated solution of Li_3N in 1 M $LiClO_4$ in EC:DMC was used as an electrolyte with a sacrificial salt to refill pouch and model cells. It should be noted

that $LiPF_6$ is required during the formation cycle and the initial cycling process to form a passivating film, in particular on the surface of aluminum foil. But since the sacrificial salt electrolyte will be added after cycling the $LiPF_6$-containing electrolyte, this should not adversely affect the aluminum foil performance.

Model experiments: Artificial Li inventory depletion as a fast ageing tool: testing of the approach.

As it can be seen from the pouch cell cycling results, very long cycling of at least 500 cycles or 2-3 months is required to significantly reduce capacity. Therefore, to more quickly develop a capacity restore method, it was necessary to develop a technique for the faster ageing of electrode materials. For this, a special cell of the “coin-cell” type was used, as shown in Figure 35a, which, unlike the coin-cell, can be easily disassembled and reassembled with a new electrolyte, and it is also possible to introduce a 3rd electrode inside this cell made of lithium metal. Commercially deposited graphite and NMC were used as electrodes and 1M LiPF6 in EC:DMC (Aldrich) was used as the electrolyte. Electrodes from pouch cells cannot be used in this cell because they are deposited on both sides of the foil. A typical discharge/charge curve of intercalation materials in this cell is shown in Figure 35b (blue curve).

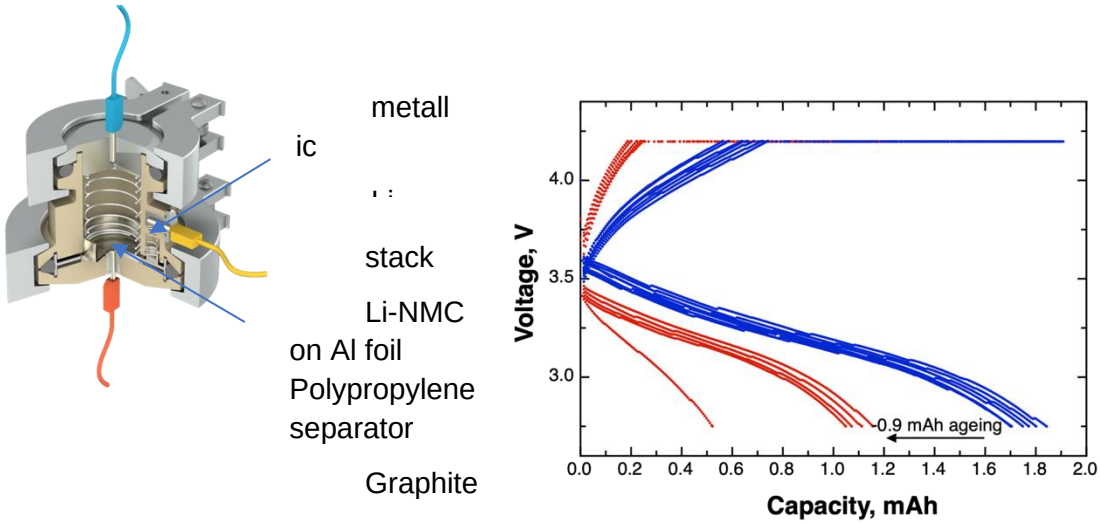

Figure 35. *(a) Scheme of a model 3 electrode “coin-like” cell. (b) Discharge/recharge voltage profiles for a model cell before and after artificial ageing.*

To carry out accelerated ageing, after stabilization discharge during 5 cycles, where graphite was used as a counter electrode and NMC as a working electrode, the cell connection scheme to the potentiostat was changed. In the course of the ageing experiments, metallic lithium was used as a counter electrode, and either graphite or NMC completely filled with lithium ions was used as a working electrode, and lithium was deposited from intercalation electrodes onto metallic lithium. Then the cell was connected according to the standard scheme: the working electrode was NMC and the counter electrode was graphite. The discharge/charge curves after the ageing process are shown in Figure 31b (red curve). The typical results of the ageing efficiency of different

intercalation electrodes are presented in Table 6. It can be seen that in all cases, after the ageing process there was a capacity decrease, but not by the charge that flowed between the lithium metal and the electrode with which the aging was carried out. The ageing efficiency is 40-85%. A possible reason for the lack of 100% efficiency is associated with the occurrence of side processes of SEI formation on the lithium metal electrode, as well as side processes on the intercalation electrodes. In principle, however, this ageing technique can be used to quickly prepare intercalation electrodes for capacity recovery experiments.

Table 6. *Efficiency of artificial ageing.*

WE during ageing	Initial capacity, mAh	Ageing charge, mAh	Capacity after ageing, mAh	Ageing efficiency, %
Graphite electrode	1,7	1,2	0,9	56
	3,9	2,7	1,4	86
NMC electrode	4,0	1,9	3,4	32
	4,5	1	4,1	40
	9,5	1	8,8	70

Refiling from a donor Li electrode (control)

To confirm the possibility to restore the intercalation electrodes capacity in a lithium-ion cell, it is necessary to demonstrate the possibility of ion intercalation in materials from the simplest source of lithium and the strongest reducing agent, metallic lithium. To do this, we used the cells described in the previous section, where a rapid aging procedure was performed before the capacity restoration procedure. To introduce lithium into the intercalation electrode, a cell connection scheme similar to the rapid ageing process was used; one of the intercalation electrodes (graphite or NMC) was used as the working electrode, and metallic lithium was used as the counter electrode. For cells where graphite was used as a working electrode, it was not possible to restore the capacity: after the procedure of capacity restoration, when measuring the cell in the standard scheme (NMC as the working electrode, graphite as the counter electrode), the capacity decreased rather than increased. More successful results were obtained in the case of capacity restoration in the NMC. An example of such capacity recovery is shown in Figure 36.

Figure 36 shows the discharge/charge curves for a cell that was first subjected to a rapid ageing procedure and then to capacity recovery using a lithium metal donor electrode. It can be seen that capacity increased by 0.2 mAh, while the charge passed through the lithium metal electrode to restore the capacity was 1 mAh. Therefore, the capacity recovery efficiency is 20%. At the same time, unfortunately, this result is poorly reproduced, and in some cases, after the process of capacity restoration for the NMC electrode, its value does not change or even decreases. This may happen if instead of the intercalation process, side processes of electrolyte decomposition and the formation of secondary SEI occur. Thus, it can be concluded that it is possible to restore capacity

using a donor electrode, but it is necessary to select the experimental conditions for this process more thoroughly.

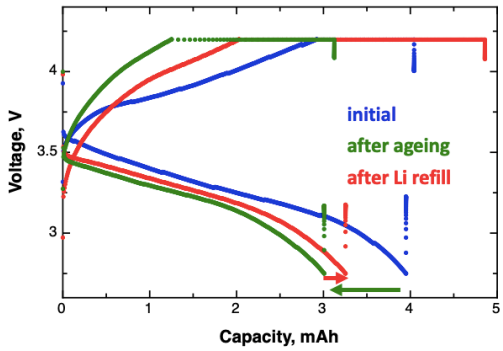

Figure 36. *Discharge/recharge voltage profiles for model cell in initial state, after artificial ageing and after Li donor electrode recovery.*

Refiling cells by Li_3N electrolyte

Our main idea to restore capacity is to use an electrolyte containing lithium nitride. At the first stage, the possibility of capacity restoration in a model cell, which was preliminarily artificially aged, was studied. Figure 37 shows the discharge/charge curves of the cell before and after adding to the cell V=200 µl of saturated Li_3N in 1M $LiClO_4$ in EC:DMC. It can be seen that capacity increased by 0.3 mAh.

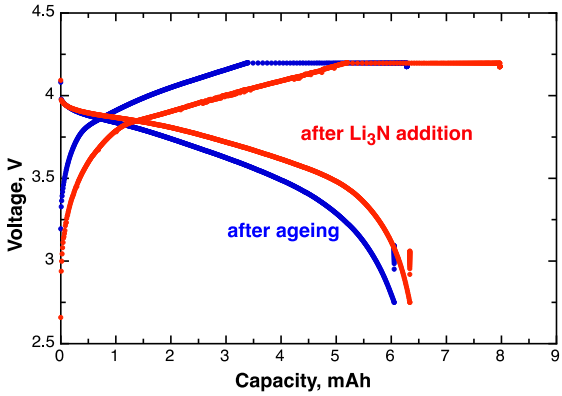

Figure 37. *Discharge/recharge voltage profiles for a model cell after artificial ageing and after refilling with the Li_3N electrolyte.*

Let us estimate the capacity value that can be recoverd. Since Li_3N is a poorly soluble compound, its expected concentration in the electrolyte is not higher than 50 mM. The oxidation of the nitride ion to nitrogen is a three-electron process:

$N^{3-} - 3e \rightarrow 1/2\ N_2$

Accordingly, the charge contained in 200 µl of the electrolyte can be estimated as Q=cVFn, where n=3, F is the Faraday number. Hence Q=2.895 C =0.8 mAh, which coincides by the order of magnitude with the observed capacity change.

Also, a lithium nitride-based electrolyte was added to the pouch cell after washing of the cells. Since (unfortunately) the number of available aged cells is currently limited, it was decided that cells that had already been washed once and filled with a conventional electrolyte will be washed again in the same way as during the first wash, then refilled with a Li_3N-saturated electrolyte based on 1M $LiClO_4$. Figure 38 shows the results of washing in various ways and refilling with electrolyte with a sacrificial salt. It can be seen that in both cases, the addition of the electrolyte with the sacrificial salt leads to a certain increase in capacity by several mAh, while this change is much smaller than after primary washing and is comparable to the change in capacity when changing the electrolyte for a slightly aged cell (Figure 28-Figure **29**). However, as mentioned earlier, a possible reason for a small increase in capacity is that the nitride content in the electrolyte is extremely low, therefore to yield an actual increase in capacity, it is necessary to pump the electrolyte with the sacrificial salt through the cell.

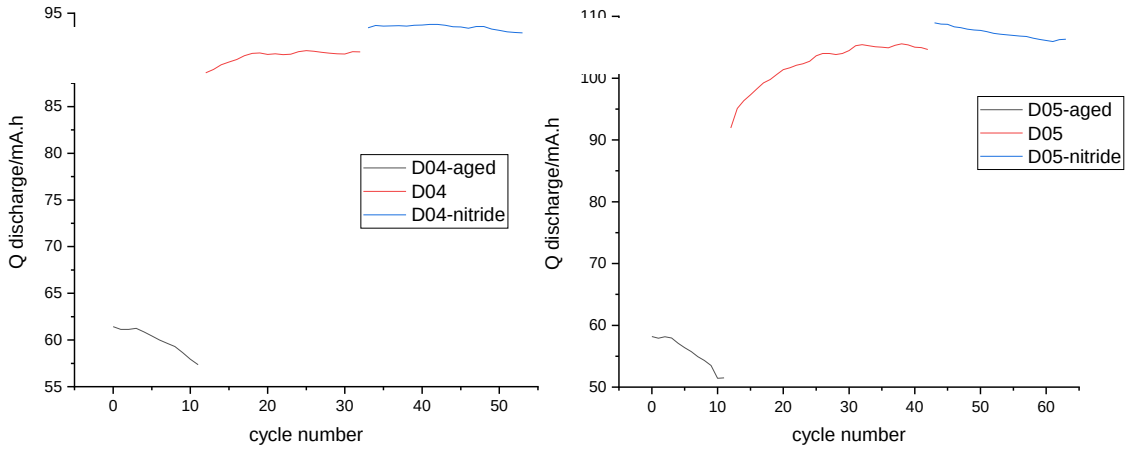

Figure 38. *Capacity vs. cycle number for an aged pouch cell that at the 1st step was washed and refilled with the ordinary electrolyte (1M $LiPF_6$ in EC:DMC) and at the 2nd step was washed and refilled with the electrolyte with the sacrificial salt (sat. Li_3N in 1M $LiClO_4$ in EC:DMC). Washing methods: (a) SC CO2+MeCN, (b) MeCN at normal pressure.*

Reproducing techniques from Kansai University

We reproduced the cell washing and electrode recovery techniques proposed by the University of Kansai.

According to the materials presented by Prof. Ishikawa's group, washing of the pouch cells at Kansai University was carried out by repeated replacement of the electrolyte using a syringe. We conducted a similar experiment. The pouch cell for this experiment was pre-cycled 10 times to control its capacity, opened using the Linecut method. Then the pouch cells were sequentially washed with a 1M $LiPF_6$ EC:DMC electrolyte (Aldrich) using a syringe with a total volume of about 1 ml, then sealed using the Linecut method. The results of cycling after sealing are shown in Figure 39. The capacity after refilling increased by 10%, which is approximately the same as the results of refilling the cells after washing by SC CO2+MeCN or MeCN. As noted earlier, the

increase in capacity may be associated with an increase in the ionic conductivity of the electrolyte and a more efficient compression of the electrodes.

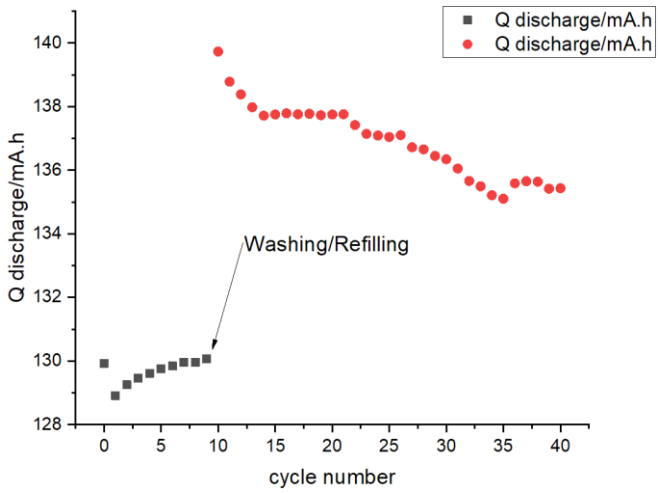

Figure 39. *Capacity vs. cycle number before and after washing/refilling by the UKansai method.*

The procedure for the NMC capacity restoration using lithium naphthalide derivatives was also reproduced. For this, a pouch cell fully charged to a voltage of 4.2V was taken, disassembled, and 6 electrodes for the coin cell were cut out of the positive electrode foil. Next, the electrodes were divided into 2 groups. One part of the electrodes (3 pieces) was kept in DME for 12 hours. The second part of the electrodes was kept in 1M 1-bromnaphtalene in DME, in which an equimolar amount of lithium was previously dissolved, also for 12 hours. Then all electrodes were rinsed by pure DME. A photo of the electrodes after removing the electrodes from the solvent is shown in Figure 40. When the electrodes were kept in pure DME, their macrostructure did not change (Figure 40a). At the same time, the formation of irregularities and bubbles is observed on the electrodes, which were kept in lithium naphthalide solution (Figure 40b,c). One of the 3 electrodes broke in halves during exposure to naphthalide. Also, on the electrodes where the capacity was restored, the formation of a yellow polymer layer was observed (Figure 40d), which could not be removed after 12 hours in pure DME.

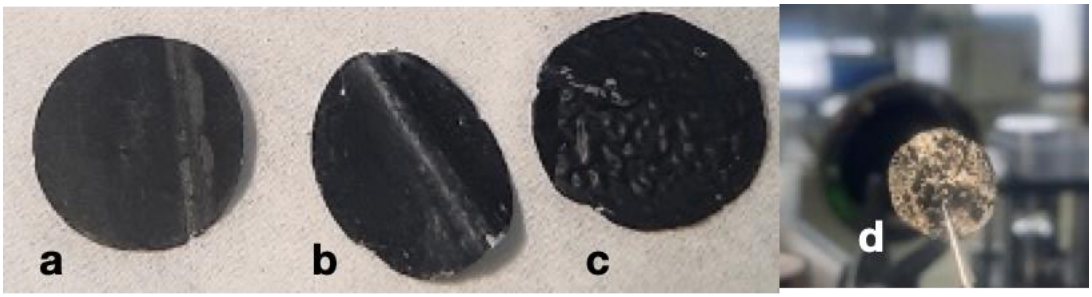

Figure 40. *Photos of NMC electrodes stored for 12 hours in pure DME(a) and in 1M 1-bromnaphtalede lithium in DME (b-d) after rinsing in pure DME.*

After washing in DME, a coin cell was assembled with all electrodes, where metallic lithium served as the counter electrode, and the electrolyte was 1M $LiPF_6$ in

EC:DMC mixture (1:1 vol., Sigma). Open circuit potential vs. time for the assembled cells is shown in Figure 41. It can be seen that the electrodes kept in lithium naphthalide have a potential below 3.2 V, which indicates that the process of lithium intercalation in NMC took place. At the same time, the potential of the electrodes that did not react with lithium naphthalide was 4.2V, i.e., the voltage to which the pouch cell was initially charged.

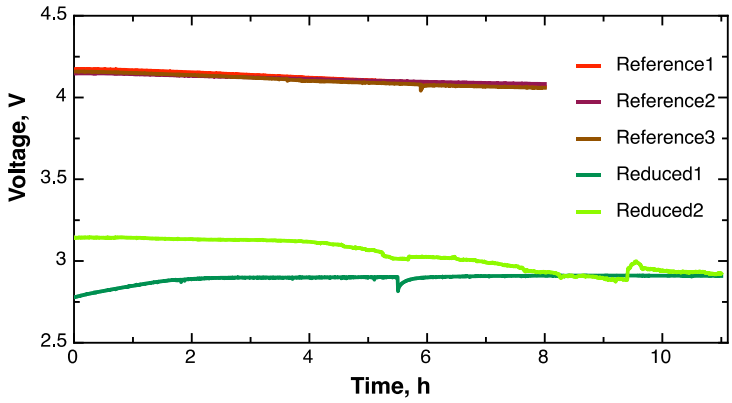

Figure 41. *Open circuit potential vs. time for coin cells with NMC kept in lithium naphthalide and in pure DME.*

At the next stage, the cycling of coin cells was carried out. Electrodes that have been kept in pure DME are reversibly discharged and charged, as illustrated in Figure 42. And the electrodes aged after lithium naphthalide during the first charge cycle showed low charge potentials, i.e. instead of lithium deintercalation, side processes occurred, possibly associated with the oxidation of polymer derivatives of lithium naphthalide side products.

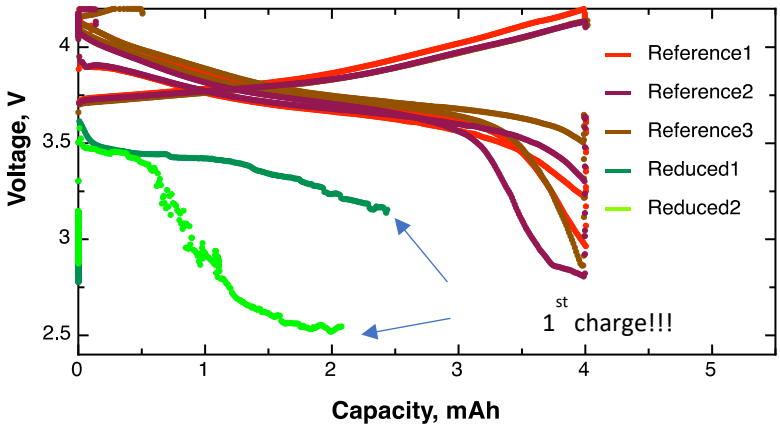

Figure 42. *Discharge/recharge voltage profiles for coin cells with NMC kept in lithium naphthalide and in pure DME.*

Thus, according to our data, Prof. Ishikawa's method does lead to lithium intercalation in the NMC. However, at the same time, mechanical destruction of the electrodes occurs alongside with the deposition of insoluble products on the surface. Perhaps the discrepancy between our results and those obtained at the University of Kansai is due to the fact that we used a different solvent, DME (not MTPH). However, in any case, it seems to us that in this method the concentration of the reducing agent is too

high, which leads to mechanical damage to the electrodes. Later, results on the capacity recovery of NMC electrodes with a lowered concentration of lithium naphthalide derivatives will be presented.

TASK 4 Cell ageing mechanisms in different ageing conditions

Literature survey on ageing of batteries in EVs

Introduction

Li-ion batteries are one of the most commonly used power sources in new energy vehicles due to their high energy density, high power density, low self-discharge rate, etc. [12]. However, to optimize the battery design and management, ageing/degradation mechanisms should be considered. It is commonly accepted that 80% of the rated capacity indicates the end of battery life in an EV [13]. The whole life cycle includes battery design, production, application in EVs, and second life application, as illustrated in Figure 43. The battery ageing and degradation should be considered even at the earliest stages of the battery life cycle, i.e., at the design and production stages. It is important to note that at different stages of the battery life cycle, different ageing/degradation mechanisms may dominate. The order in which the various degradation mechanisms are triggered also depends on the usage patterns, i.e., the time of battery being at rest (during the vehicle parking) or cycled.

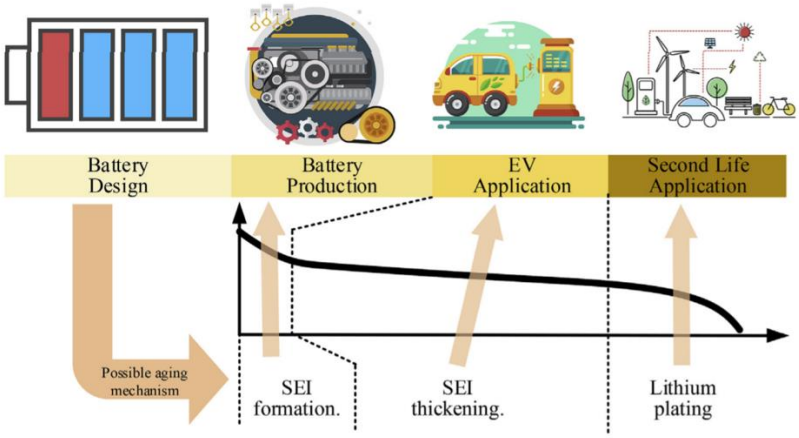

Figure 43. *Battery life cycle: design, production, EV application, and second life application* [14].

Another important factor that needs to be taken into account is battery design, which directly influences the respective ageing/degradation mechanisms and phenomena. Here, several levels of the battery design should be taken into account, as illustrated in Figure 44: the lowest material level, the electrode level, the cell level, and the system level. The factors between various levels can also be interrelated (for example, SEI formation, heat generation and dissipation, etc. [12,14]). Ageing at the material level usually influences the cathode, anode, electrolyte, and/or separator materials and thus strongly depends on their nature; in addition, coating, doping, etc. can also influence the ageing mechanisms

[15]. Design at the electrode level usually features the anode/cathode active material ratio, electrode particle size, porosity, electrode thickness, etc. [14]. An optimized electrode-level design can strongly influence battery ageing due to the reduction of mechanical factors (stress), electrical factors (polarization), and thermal factors (temperature). For example, usually, the anode active material is taken in slight excess [16], and insufficiency of anode material can lead to increased risks of degradation through lithium plating, which results in capacity fade and safety problems [17]. Design at the cell level usually refers to the type of the cell internal structure (stacked or wound), the cell shape (cylindrical, prismatic, or pouch), cell size, etc. Since these choices are mainly restricted by the production equipment, standards, design, EV requirements, etc., this factor will not be considered in this survey. Finally, the system level ageing issues, which are associated with mechanical, electrical, and thermal effects of cells integration into a battery system, should also be taken into account. The battery stack/system ageing is mainly influenced by the thermal management system (TMS) and battery management system (BMS). Another important factor is the compressive pressure load on the cells [18,19]. In this survey, we will mainly focus on the material level ageing and also briefly review the influence of the battery working conditions on their ageing/degradation as well as the current approaches to battery pack ageing studies.

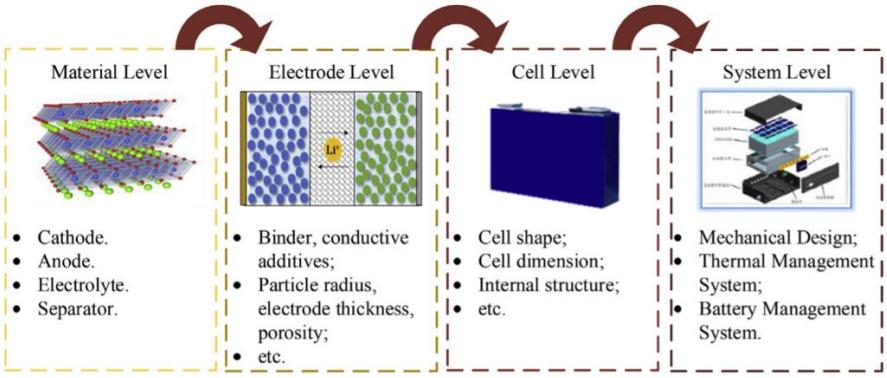

Figure 44. *Battery design at different levels [14]*

Principal ageing/degradation mechanisms

At the material level, the main ageing/degradation mechanisms are **loss of lithium inventory** (**LLI,** leading to reduction of the amount of cyclable lithium available for transport between the electrodes) and **loss of anode/cathode active materials** (**LAM,** i.e., reduction in the quantity of material available for electrochemical activity**)**, which can happen at both cathode and anode**.** These mechanisms can be described by the dual-tank model as illustrated in Figure 45 [20]. In addition, the degradation can also cause internal resistance increase (RI, also called impedance rise), loss of electrolyte (LE, including the loss of additives; it can often lead to RI and eventually to LAM), and stoichiometric drift, when the electrodes become imbalanced relative to each other. All ageing modes are caused by certain internal physical or chemical processes, as illustrated in Figure 46 and Figure 47. Apart from the aforementioned processes, salt precipitation, current collector corrosion, binder decomposition, separator pore blockage, electrode-current collector delamination can take place [14]. In this study, we focus mainly on the mechanisms that involve either anode or cathode materials. It should be noted that

it is difficult to directly observe any of these mechanisms during the battery operation, they are rather studied post-mortem after the cell/battery is disassembled; the effects that can be directly observed during battery operation are capacity fade and power fade [21].

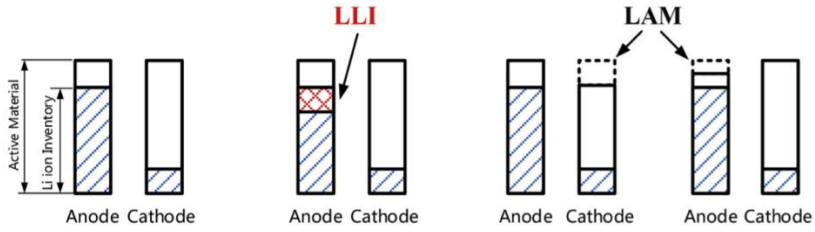

Figure 45. *Illustrations of the LLI and LAM mechanisms of Li-ion cell ageing/degradation [20].*

In brief, generally speaking, LAM is often caused by graphite exfoliation, metal dissolution coupled with electrolyte decomposition, collector corrosion, binder decomposition, etc. LLI may be caused by the SEI formation and development, lithium deposition, etc. LE may be caused by electrolyte consumption in side reactions like SEI film thickening, electrolyte decomposition at high potentials, etc. Finally, RI can be caused by SEI formation and thickening, LE, etc. The basic physical and chemical processes that cause the corresponding ageing modes are summed up in Figure 47.

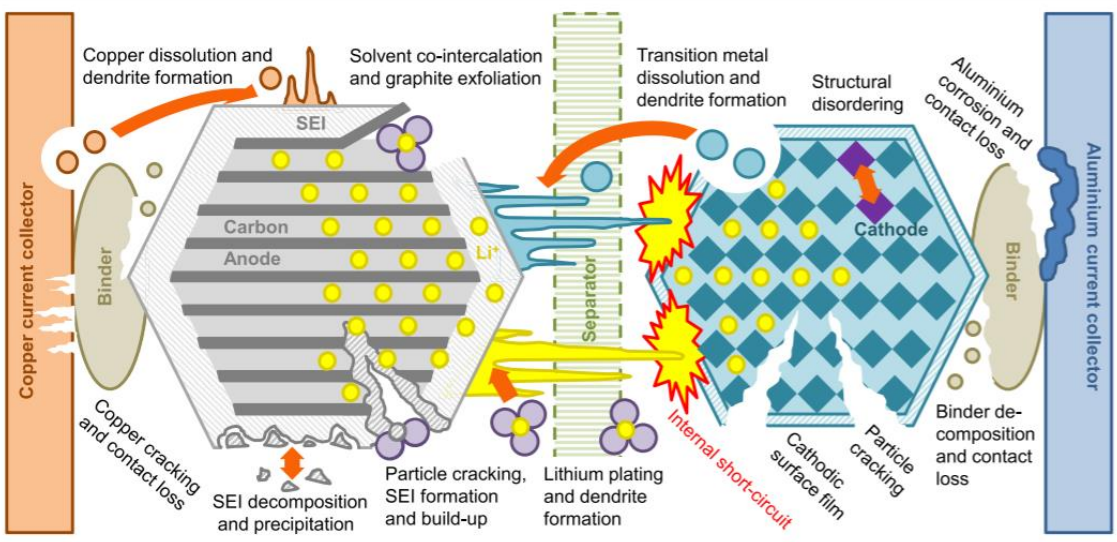

Figure 46. *The main ageing/degradation mechanisms in Li-ion cells used in EVs [22].*

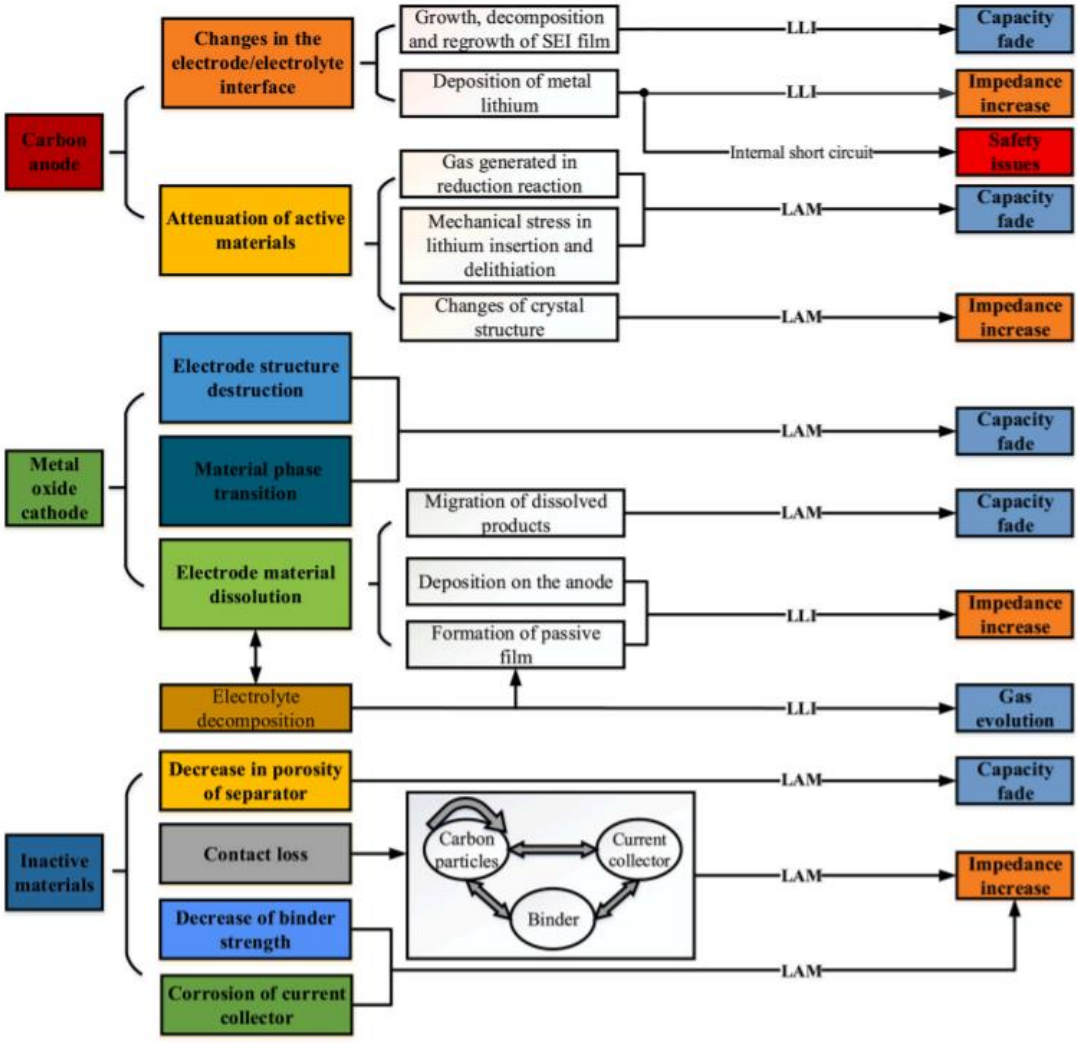

Figure 47. *Basic physical processes and chemical reactions inside a battery, the corresponding ageing/degradation modes (LAM/LLI) and the resulting effect on the cell performance [23].*

The ageing/degradation mechanisms are material-dependent. Currently, there are many kinds of commercial intercalation materials that can be used in lithium-ion power batteries for electric vehicles [24]. Most of the internal ageing reactions happen at the anode and the cathode. Some typical cathode materials include lithium manganese oxide (LMO, $LiMn_2O_4$), lithium iron phosphate (LFP, $LiFePO_4$), layered metal oxide like $Li[Ni_xCo_yMn_{1-x-y}]O_2$ (NCM), and Li-rich materials. And the anode materials include graphite (C), $Li_4Ti_5O_{12}$ (LTO), and Si. At present, there are only several kinds of Li-ion cells with specific anode and cathode combinations including LFP/C, LMO/C, NCM/C, NCM/LTO, etc. LFP/C cell has a long life and high safety, but low energy density and low power density. LMO/C cells have higher energy density and power density, but poor life characteristics. NCM/C cells have high energy density and poor safety; it is mostly used in pure electric vehicles, especially in passenger cars. NCM/ LTO cells have high power performance, high safety, and long life, but low energy density due to the low voltage; for this reason, they are often used in fast charging vehicles and hybrid vehicles [12].

Ageing of the anode materials. The anode materials are subject to both LLI and LAM. As most commercial Li-ion batteries use carbon-based anodes (usually graphite-based), and the graphite anode is theoretically unstable, a protective passivation layer usually called SEI is used to facilitate lithium-ion transport while preventing electron transportation. The SEI is formed during the first few charging processes, especially during the first cycle; its formation and further evolution are due to LLI and result in capacity fade [25]. Due to the volume change during charging/discharging, the SEI film may crack, which leads to the contact and reaction between the lithiated graphite and the electrolyte, thus causing continuous generation and thickening of the SEI film throughout the whole battery life cycle. This process is widely recognized as one of the major reasons behind the Li-ion battery ageing [26,27]. It should be noted that the SEI growth rate approximately correlates with the square root of time [28], and the SEI layer grows even when the battery is not being used. However, high temperatures and high currents promote SEI growth. The onset of SEI formation is not fixed, it depends on the electrolyte composition, the content of additives, etc. The formation of an SEI film is a set of competing or promoting reactions with complex interrelation [26]. For this reason, the SEI composition is complex and it is believed to include inorganic components (i.e., salt degradation/decomposition products) and organic components (electrolyte solvent reduction products) [29]. The SEI stability, composition, and structure depend on the composition of the electrolyte and the electrode, as well as on certain external factors (mainly current and temperature). In order to postpone the battery ageing, electrolyte additives and anode surface modification are used [30]. If LTO is used as the anode material, there is no SEI formation as the electric potential is within the electrolyte stabilized window. Another popular anode material, silicon, is prone to SEI film formation; continuous thickening of the SEI film would lead to irreversible LLI. Due to the dramatic expansion of silicon during lithiation, SEI cracking and subsequent recreation may cause loss of contact with the current collector [31]. For these reasons, many researchers focus on Si/C composite anode materials.

Another predominantly LLI-based ageing mechanism is metal lithium deposition at the graphitic anode (Li plating), which is usually observed under extreme conditions such as overcharging or charging at high rates. This process may also cause loss of electrolyte (LE) [17]. The deposited lithium is associated with a number of negative effects such as increased anode polarization, hindered anode performance, generation of side reaction products, short circuits due to lithium dendrites, thus ultimately presenting a source of safety hazard [32]. It should be noted that LTO-based anodes are not subject to this ageing mechanism due to the relatively high potential.

The third ageing/degradation pathway mainly observed for graphite-based anodes is graphite exfoliation due to the active material volume change during intercalation/deintercalation or due to co-intercalation of Li ions and the solvent molecules, generation of gas particles (such as CO or H_2) during anode reduction reactions, or changes in the crystal structure (which all lead to LAM and capacity fade or impedance increase); again, this mechanism is irrelevant for LTO-based anodes as LTO is a zero-strain material [33]. Graphite exfoliation inevitably causes the new SEI film generation as described above. Finally, LAM can also happen due to current collector corrosion and binder decomposition (see Figure 46).

Ageing of cathode materials. At present, most commercial power lithium-ion batteries in EVs use LMO, LFP, or NCM cathode materials as described above. The cathode ageing, in general, happens either through LAM or through LLI mechanisms. The main LAM mechanisms are through electrode structure destruction or due to material phase transition; they inevitably cause capacity fade. LLI takes place due to electrode material dissolution, i.e., migration of dissolved products, their deposition on the anode, and formation of a passivating film. The latter causes an impedance increase. Similar to the anode, a passive film called cathode electrolyte interface (CEI) can appear due to the oxidation of the electrolyte and LiPF6 decomposition during the first and subsequent charging. CEI is mostly composed of $ROCO_2LI$, polycarbonates, and LiF [34]. The CEI film is usually thinner than SEI and, in contrast to it, does not fully cover the cathode surface

In detail, the LMO cathode material is widely used for EVs due to its low price, high energy density, and non-toxicity. The main ageing mechanisms related to this type of cathode are LMO associated with structural deformations caused by the Jahn-Teller distortions (causing phase transformations of LMO from cubic to tetragonal [35], which can generate mechanical stress) and Mn dissolution due to either Mn^{3+} disproportionation, especially at low potential (leading to Mn^{2+}, which is soluble in the electrolyte and can be replaced with Li ions), or HF dissolution of manganese. In addition to LAM, Mn dissolution also leads to loss of electrolyte (LE), SEI growth, and CEI formation (at high potentials). For batteries with low potential anode like graphite, the manganese ions may move through the separator and be reduced on the anode surface; which may cause the SEI thickening and result in accelerated LLI and resistance increase (also due to CEI growth) [36]. However, for batteries with higher potential anode like LTO, the manganese ions will not be reduced, and the battery cycle life can be effectively improved [37].

The LFP cathodes have low voltage and high resistance, which results in low energy density. However, certain advantages are associated with the use of this cathode in EVs, which are: long cycle and storage life, low price, and safety, which makes it very attractive especially for commercial EVs. In the case of LFP, the LAM effect due to iron dissolution in the electrolyte is less pronounced than for LMO, and less CEI is formed; the iron ions may also be reduced on the anode surface and catalyze the SEI formation, resulting in increased internal resistance and LLI [38].

The layered NCM cathodes have high energy density and low price, which has been widely used in passenger EVs. The battery performance and the ageing mechanism strongly depend on the cathode composition, i.e., on the Ni, Co, and Mn proportion. In general, higher Ni content leads to higher capacity but smaller cycle life and less thermal stability, higher Mn content yields good cycle life and safety but is also associated with Mn dissolution as discussed above, while higher Co content leads to lower resistance and improved power performance. The main ageing mechanism for the NCM cathodes includes volume change during charging/discharging; dissolution of Ni/Co/Mn ions in the electrolyte; and CEI generation due to side reactions between the cathode materials and the electrolyte [39,40]. Both SEI growth and CEI formation cause resistivity increase. No Jahn-Teller effect typical for LMO is involved. For the Ni-rich NCM materials, the cation mixing phenomena becomes more distinct, and phase transformations are more likely to

happen, yielding high mechanical stress and irreversible capacity deterioration. High temperatures accelerate the cathode degradation rate through all mechanisms listed above [21].

Ageing of other battery parts. Reactions in other parts of batteries occur on inactive materials such as current collectors, separators, conductive agents, and binders (see Figure 47). The most typical reactions are binder and collector corrosion (leading to resistance increase and contact loss between active materials, thus triggering the LAM ageing mechanism), a decrease of the separator porosity causing less ion through-rate and capacity fade [41], self-discharge during battery storage due to many factors such as internal or external electron leakage, electrolyte leakage, electrode/electrolyte reactions, partial dissolution of active material, electrode passivation, and mechanical decomposition [42]. The LLI ageing mechanism dominates the performance degradation during storage [43].

The interrelation and mutual triggering of the ageing mechanisms. It is important to note that different ageing mechanisms are interrelated, can trigger each other or compete, therefore they should not be considered as isolated phenomena. Figure 48 illustrates the complex interrelation between various ageing mechanisms and phenomena. However, thorough studies of such interrelations are rare, e.g., in [44] it was demonstrated that the growth of the SEI film leads to pore blockage, which causes further Li plating rate increase and results in non-linear cell capacity fading. Another example is SEI growth due to mechanical fracture of the anode and transition metal dissolution from the cathode [45]. It has also been shown that mechanical fracture can be self-reinforcing.

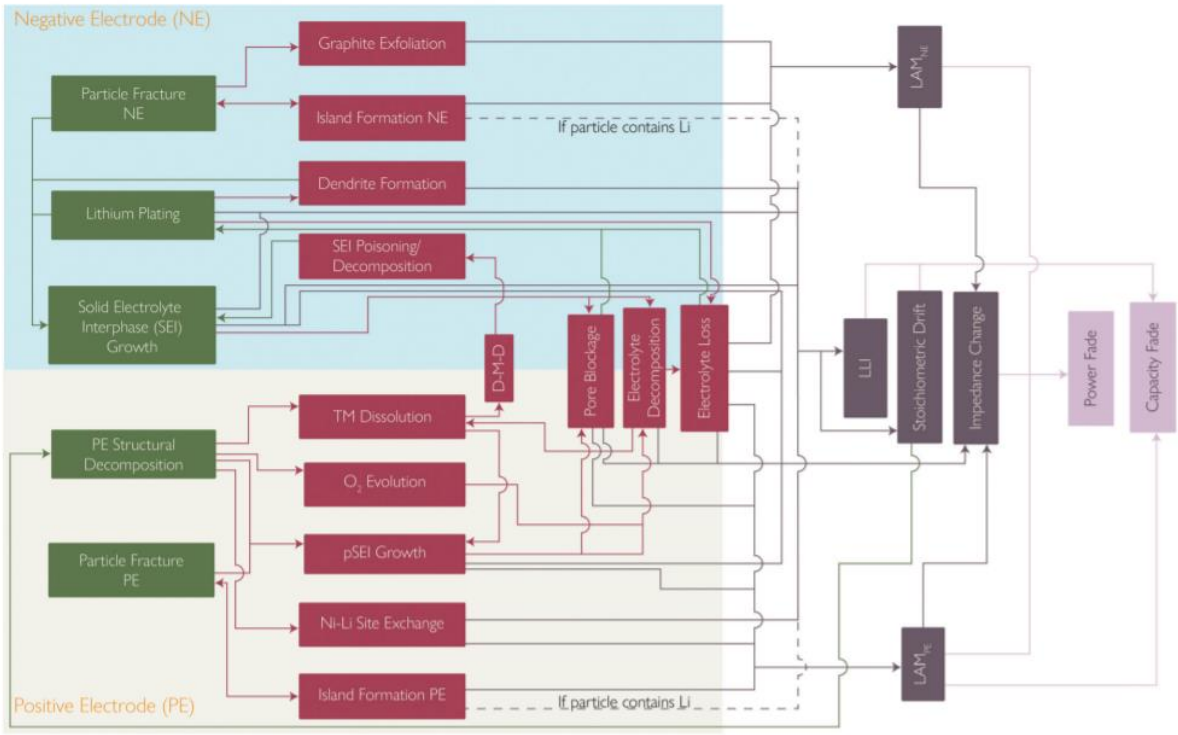

Figure 48. *Interplay between primary and secondary ageing/degradation mechanisms and their influence on the cell performance [21].*

The dominating ageing/degradation mechanism also changes within the battery life cycle. Figure 49 shows possible internal mechanisms for the battery capacity fade during its life cycle. At the initial stage, the SEI layer is being formed; after that, during the main part of the battery use, the SEI layer grows continuously, while the cathode material undergoes structural transformations, and the electrolyte is lost in many processes (occuring at both cathode and anode as described above). Finally, at the last stage capacity starts to fade quickly due to lithium plating domination and contact loss of active materials, which is mainly caused by LE, volume changes/structural transformations and binder corrosion.

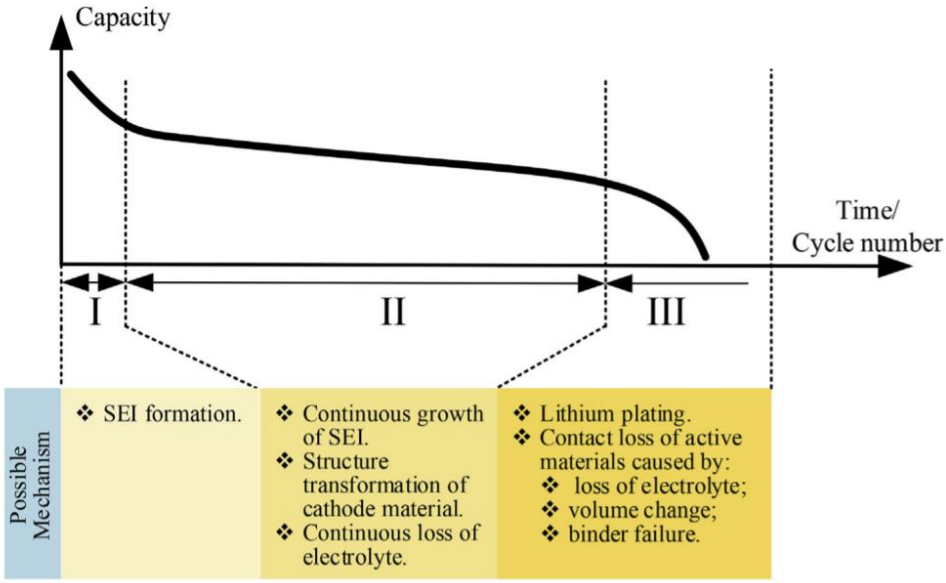

***Figure 49**. Battery capacity fade and possible internal mechanisms at different stages [14].*

Influence of the battery operating conditions on their ageing/degradation

The main external factors that affect battery ageing are operating temperatures (with both too high and too low temperatures being a negative factor), high state-of-charge (SOC)/overcharge or low SOC/over-discharge, and high charge/discharge rates. Temperature is one of the most important factors that may affect battery degradation/ageing [46]: at high temperatures, side reactions are accelerated, while at low temperatures the main risks are lithium deposition and active material structure damage. Generally, for most commercial Li-ion batteries the optimal operating temperature range is 15-35^{0}C. For the actual EVs, the most common state is parking, when the battery temperature equals the environment temperature, which can also significantly influence the battery ageing. Temperature variations cause both LLI and LAM ageing mechanisms (see Figure 50). Overcharge causes risks of electrolyte decomposition, side reactions between the electrolyte and the cathode, as well as Li-ion

deposition [47] mostly through LLI, while over-discharge can lead to current collector corrosion and collapse of the active material structure [48] predominantly through LAM. High charge and discharge rates can cause fatigue or damage in the crystal structure of the active material, as well as accelerate side reactions due to the associated temperature rise [49]. Most of the external factors that influence the ageing mechanisms and modes are summed up in Figure 50.

Certain measures can be undertaken to postpone battery ageing. From the internal perspective, the use of additives to the electrolyte is one of the most promising approaches; it helps suppress certain ageing reactions. Other approaches involve coating of the cathode active particles, reducing the electrode loadings, or replacing natural graphite with an artificial one. The external factors that promote ageing are extreme temperatures, large charge/discharge rates, and high depth of discharge. The ageing mechanisms also strongly depend on the cutoff voltage of charge and discharge and the operating window of the cell.

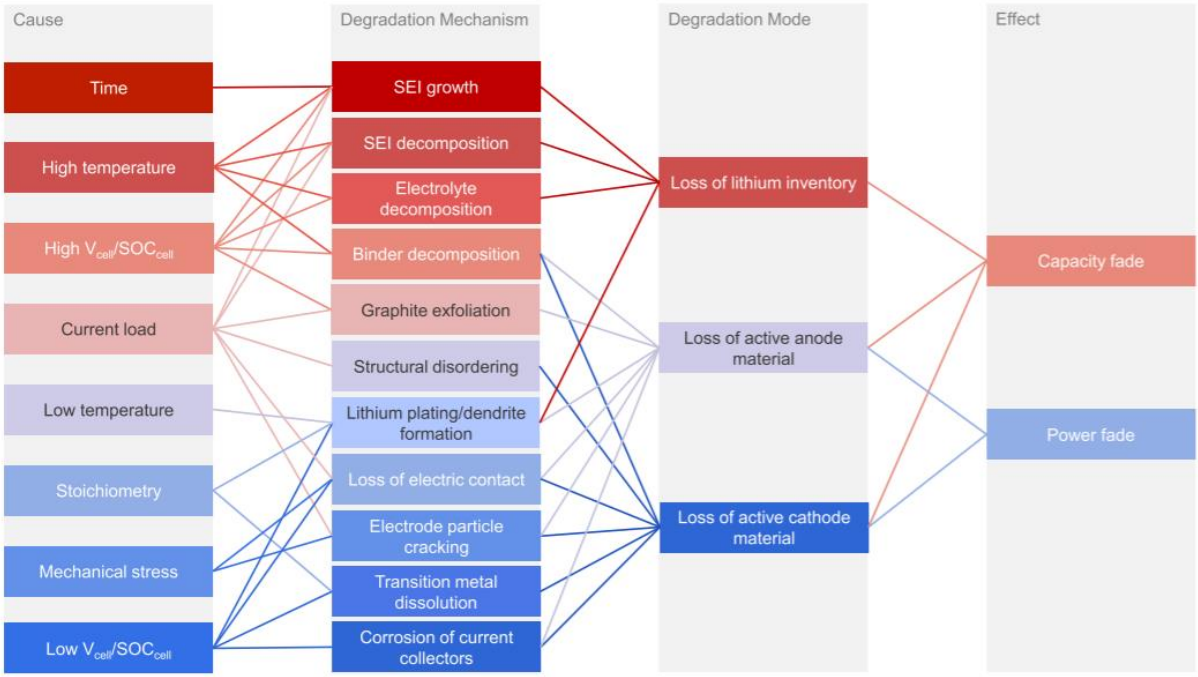

Figure 50. *Interconnection between the operating conditions/external factors, the ageing/degradation mechanisms, and the associated ageing/degradation modes [22].*

Ageing mechanisms of battery systems/packs

To date, most of the ageing studies refer to single cells rather than battery packs or systems. This is caused by two primary factors: first, the performance of a pack/system is to a great extent determined by a single cell performance, therefore the system ageing is greatly influenced by the ageing phenomena within each individual cell. Second, the battery performance is greatly affected by the inconsistency between the cells [14]. The approaches to the analysis of battery system ageing mainly include pack status histograms or electric quantity–capacity scatter diagrams [50,51].

Methods for ageing diagnosis and prognosis

There are three main groups of diagnosis methods used to determine the underlying ageing/degradation mechanisms for the batteries used in EVs: post-mortem analysis of disassembled cells/batteries, curve-based analysis, and model-based analysis.

Post-mortem analysis includes various methods of physicochemical analysis, which can be divided into three main groups [23]: (1) morphology analysis, for example, SEM, optical microscopy, TEM, etc; (2) composition analysis, for example, EDX, XPS, ICP-AES; and (3) structural analysis, mainly by XRD and related methods. The methods can be applied either *in-situ* or *ex-situ* [52]; sometimes analytical techniques are also used *operando*, thus no cell disassembly is required.

The curve-based analysis includes incremental capacity analysis (ICA) and differential voltage analysis (DVA) based on the battery OCV curves. The curves are mathematically transformed to derive the underlying ageing/degradation mechanisms [23].

There are two general approaches to modeling: (1) empirical modeling, when an incremental process is used to apply equations and parameters in order to achieve the best fit to experimental data (while the equations may not have any real meaning), and (2) physics-based modeling, where the simulated behavior is derived from equations that are known to represent the actual physical behavior involved. The approaches used at different levels (from the molecular scale to battery packs) are illustrated in Figure 51. The empirical models mainly focus on the cell and pack levels; they include, for example, equivalent-circuit models (ECM), which describe the electrical behavior of a battery using a set of circuit elements such as resistors and capacitors. However, empirical models are not very well suited for degradation/ageing mechanisms as they often assume a regular daily charging pattern. A combination of experimental data and ECM is realized in electrochemical impedance spectroscopy (EIS), where the EIS spectrum is obtained for an operating cell and can be described by an ECM. Different battery ageing modes, i.e., LLI, LAM, and RI, are described by different sets of circuit elements, as illustrated in Figure 52.

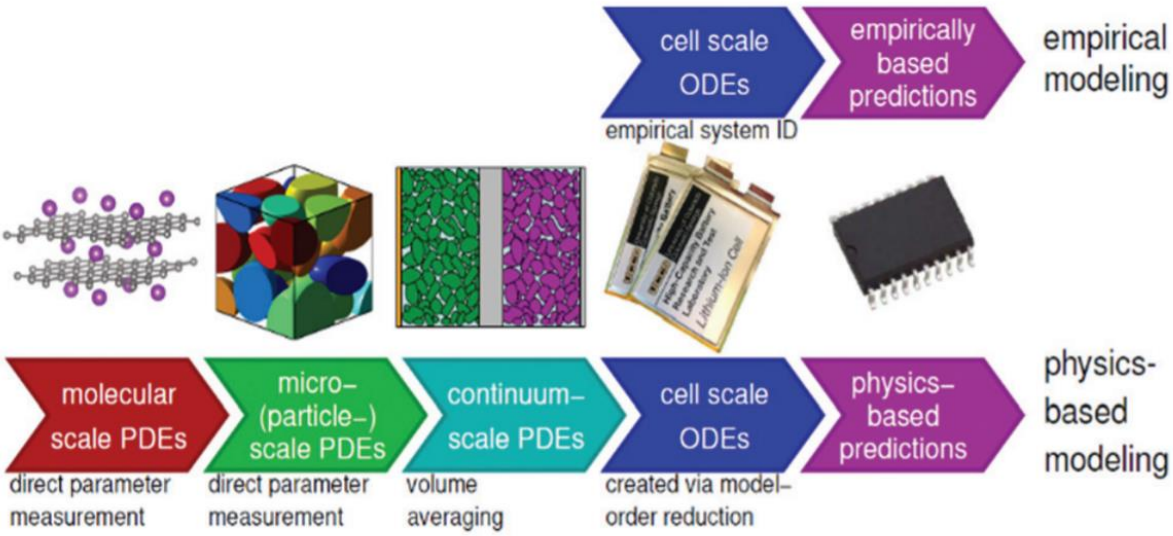

Figure 51. *Battery modeling at various levels [21].*

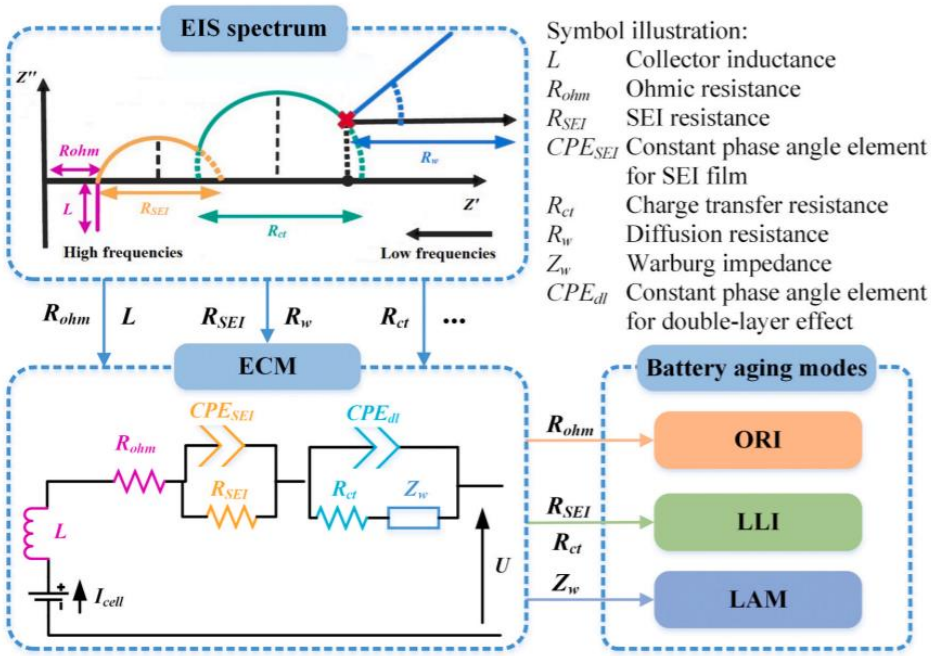

Figure 52. *Application of EIS to identify the battery internal ageing/degradation mechanisms/modes [53].*

The physics-based models use a set of coupled partial differential equations (PDEs) to model electrochemical and chemical interactions within a battery. Different processes responsible for the ageing/degradation can be described by specific equations as illustrated in Figure 53. The physics-based approach can be applied at various scales, starting from the molecular level and going up to the battery pack level. The values derived at each scale can be used as input parameters for higher scales. Typically, these models describe the charge and mass conservations in the homogeneous solid and electrolyte, as well as the lithium flux between the solid and electrolyte phases. Digital

simulation of the physics-based models requires a discretization in space and time. At the atomistic scale, no universal framework exists for simulating degradation mechanisms, but classical molecular dynamics (MD), mesoscopic modeling, and ab initio density functional theory (DFT) have been used to investigate the origin and effects of cracking and stresses in Si anodes during charge [54] and techniques for understanding cathode degradation have been recently reviewed. Doyle, Fuller, and Newman have developed the widely used electrochemical model including mass conservation, charge conservation, and reaction kinetics [55,56]. While this model can provide a comprehensive analysis of the internal dynamics of a battery, discretizing and solving a physics-based model in both dimensions often result in hundreds or even thousands of equations. Therefore, implementing a physics-based model for real-time BMS monitoring is computationally expensive.

Hybrid approaches are also being used, where simplified techniques are used to yield a quicker yet accurate physics-based description of the battery behavior. Such hybrid approaches include, for example, mechanistic models [57] and single-particle models (SPM), in which each electrode domain is simplified into a single spherical particle [58]. These approaches yet have limitations, for example, SPMs are usually limited to low-current applications, which constrain the use of such models for fast-charging in an electric vehicle. However, recently novel SPM approaches have been proposed, which include the electrolyte dynamics as well as the SEI layer formation [59].

Recently in addition to the diagnosis, ageing prognosis has also come into focus since it helps predict the dominating ageing mechanism and ensure the safety of battery operation [23].

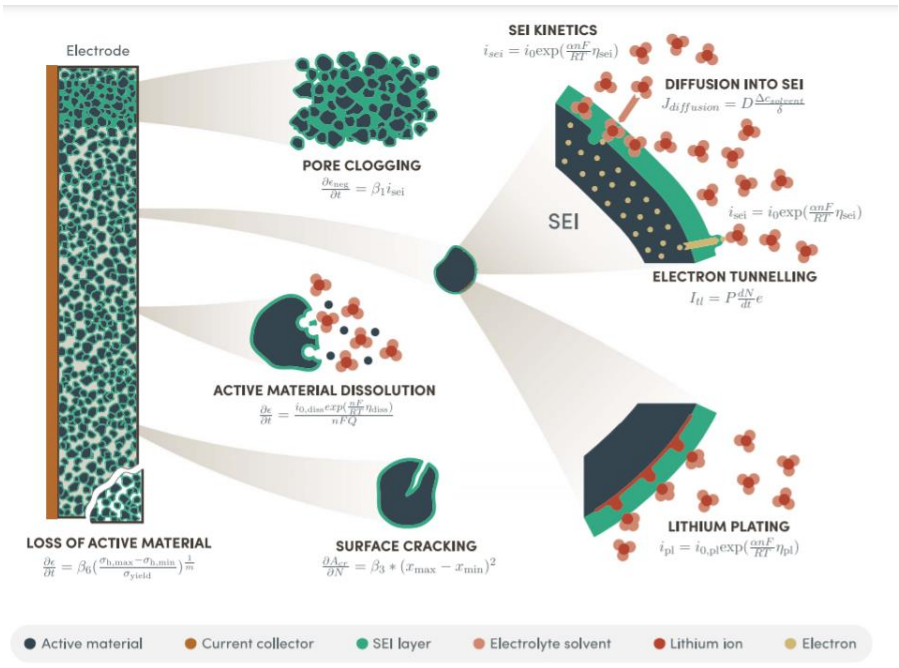

Figure 53. *Illustration of the various degradation mechanisms with typical equations modelling each mechanism [60].*

Conclusions

- A new version of HPEC with an O-ring was produced. Corrosion was eliminated. The new HPEC design with a copper pressed current collector was produced. Cycling of the new HPEC is better than for the previous versions but is not good enough yet for the next research actions with HPEC.
- A technique for pouch cell washing by supercritical fluids and pure solvents under conditions that are as similar as possible was established. According to the ICP AES data, electrolyte washing efficiency by SC CO_2+MeCN and MeCN at normal pressure is the same for both slightly aged and deeply aged pouch cells. The amount of extracted lithium for deeply aged cells is 2 times smaller.
- The SEI layer was studied by ToF-SIMS, FTIR, and SEM. It was found that there is no strong difference in the SEI thickness/morphology for different washing procedures (either by SC CO_2+MeCN or MeCN) and both for slightly aged and deeply aged pouch cells.
- According to the XRD analysis, the washing procedure does not change the material structure.
- A reproducible pouch cell opening/resealing procedure was established and tested. Slightly aged pouch cells that were washed either with SC CO_2 + MeCN or with MeCN and refilled with the ordinary electrolyte show the same capacity that they had before the washing.
- Washing of deeply aged pouch cells either with SC CO_2+MeCN or MeCN at normal pressure and their subsequent filling with the ordinary electrolyte (**without** any sacrificial salt added) leads to an **increase** in the discharge capacity of the cells.
- Model cells with an additional Li electrode could be aged artificially; in principle, their capacity may be restored using a Li metal donor electrode.
- Li_3N is the best sacrificial salt candidate among other oxidizable Li salts and tested organic compounds. Li_3N doesn't dissolve in a $LiPF_6$-based electrolyte.
- The use of the Li_3N-based electrolyte could help restore the capacity in either model or pouch cells. But the nitride content in the electrolyte is extremely low, so to yield an actual increase in capacity it is necessary to pump the electrolyte with the sacrificial salt through the cell.
- UKansai methods for pouch cell washing and NMC capacity recovery were re-checked. The electrochemical performance of a pouch cell after washing with the electrolyte remains almost the same. The method of NMC recovery leads to an increase in Li concentration in NMC but at the same time the macrostructure of the electrodes was destroyed, they were covered by an insoluble polymer film that prevents cycling of restored electrodes.

Outlook

Based on the results obtained so far, our group has elaborated a number of approaches to further improve the HPEC design. Furthermore, we would like to perform ToF-SIMS experiments with improved conditions (zero air exposure of the samples,

negative+positive modes combined, deciphering of the SEI composition based on the attribution of the spectral lines etc.) in order to shed more light on the SEI composition and washing influence.

Regarding the sacrificial salts studies, we established that Li_3N can be used as recovery electrolyte, however, it appears that a system for electrolyte purging should be developed to further investigate this topic. Finally, we believe that the UKansai recovery procedure could be improved by decreasing the concentration of the doping solution.

References

[1] D. Aurbach, Review of selected electrode–solution interactions which determine the performance of Li and Li ion batteries, J Power Sources. 89 (2000) 206–218. https://doi.org/10.1016/s0378-7753(00)00431-6.

[2] E. Kuzmina, E. Karaseva, A. Ivanov, D. Kolosnitsyn, S. Mochalov, R.V. Kumar, V. Kolosnitsyn, Mitigating strategy in lithium dendrite formation in a Li–S cell in accelerated cycling tests, Electrochim Acta. 327 (2019) 135007. https://doi.org/10.1016/j.electacta.2019.135007.

[3] J.T. Lee, N. Nitta, J. Benson, A. Magasinski, T.F. Fuller, G. Yushin, Comparative study of the solid electrolyte interphase on graphite in full Li-ion battery cells using X-ray photoelectron spectroscopy, secondary ion mass spectrometry, and electron microscopy, Carbon. 52 (2013) 388–397. https://doi.org/10.1016/j.carbon.2012.09.049.

[4] N. Saqib, C.M. Ganim, A.E. Shelton, J.M. Porter, On the Decomposition of Carbonate-Based Lithium-Ion Battery Electrolytes Studied Using Operando Infrared Spectroscopy, J Electrochem Soc. 165 (2018) A4051–A4057. https://doi.org/10.1149/2.1051816jes.

[5] D. Aurbach, B. Markovsky, I. Weissman, E. Levi, Y. Ein-Eli, On the correlation between surface chemistry and performance of graphite negative electrodes for Li ion batteries, Electrochim Acta. 45 (1999) 67–86. https://doi.org/10.1016/s0013-4686(99)00194-2.

[6] G.G. Eshetu, S. Grugeon, G. Gachot, D. Mathiron, M. Armand, S. Laruelle, LiFSI vs. LiPF6 electrolytes in contact with lithiated graphite: Comparing thermal stabilities and identification of specific SEI-reinforcing additives, Electrochim Acta. 102 (2013) 133–141. https://doi.org/10.1016/j.electacta.2013.03.171.

[7] N.R.C. Egypt Inorganic Chemistry Department, A.M. Hashem, R.S. El-Tawil, M. Abutabl, C.U. Egypt Department of Physical Chemistry,, A.E. Eid, Pristine and coated LiNi1/3Mn1/3Co1/3O2 as positive electrode materials for li-ion batteries, Res Eng Struct Mater. 1 (2015). https://doi.org/10.17515/resm2015.07en0315.

[8] N. Ehteshami, L. Ibing, L. Stolz, M. Winter, E. Paillard, Ethylene carbonate-free electrolytes for Li-ion battery: Study of the solid electrolyte interphases formed on graphite anodes, J Power Sources. 451 (2020) 227804. https://doi.org/10.1016/j.jpowsour.2020.227804.

[9] J.T. Lee, N. Nitta, J. Benson, A. Magasinski, T.F. Fuller, G. Yushin, Comparative study of the solid electrolyte interphase on graphite in full Li-ion battery cells using X-ray photoelectron spectroscopy, secondary ion mass spectrometry, and electron microscopy, Carbon. 52 (2013) 388–397. https://doi.org/10.1016/j.carbon.2012.09.049.

[10] H. He, C. Huang, C.-W. Luo, J.-J. Liu, Z.-S. Chao, Dynamic study of Li intercalation into graphite by in situ high energy synchrotron XRD, Electrochim Acta. 92 (2013) 148–152. https://doi.org/10.1016/j.electacta.2012.12.135.

[11] I. Buchberger, S. Seidlmayer, A. Pokharel, M. Piana, J. Hattendorff, P. Kudejova, R. Gilles, H.A. Gasteiger, Aging Analysis of Graphite/LiNi 1/3 Mn 1/3 Co 1/3 O 2 Cells Using XRD, PGAA, and AC Impedance, J Electrochem Soc. 162 (2015) A2737–A2746. https://doi.org/10.1149/2.0721514jes.

[12] L. Lu, X. Han, J. Li, J. Hua, M. Ouyang, A review on the key issues for lithium-ion battery management in electric vehicles, J Power Sources. 226 (2013) 272–288. https://doi.org/10.1016/j.jpowsour.2012.10.060.

[13] T.Q. Duong, USABC and PNGV test procedures, J Power Sources. 89 (2000) 244–248. https://doi.org/10.1016/s0378-7753(00)00439-0.

[14] X. Han, L. Lu, Y. Zheng, X. Feng, Z. Li, J. Li, M. Ouyang, A review on the key issues of the lithium ion battery degradation among the whole life cycle, Etransportation. 1 (2019) 100005. https://doi.org/10.1016/j.etran.2019.100005.

[15] Y.-K. Sun, Z. Chen, H.-J. Noh, D.-J. Lee, H.-G. Jung, Y. Ren, S. Wang, C.S. Yoon, S.-T. Myung, K. Amine, Nanostructured high-energy cathode materials for advanced lithium batteries, Nat Mater. 11 (2012) 942–947. https://doi.org/10.1038/nmat3435.

[16] J. Christensen, J. Newman, Cyclable Lithium and Capacity Loss in Li-Ion Cells, J Electrochem Soc. 152 (2005) A818. https://doi.org/10.1149/1.1870752.

[17] Z. Li, J. Huang, B.Y. Liaw, V. Metzler, J. Zhang, A review of lithium deposition in lithium-ion and lithium metal secondary batteries, J Power Sources. 254 (2014) 168–182. https://doi.org/10.1016/j.jpowsour.2013.12.099.

[18] A. Barai, R. Tangirala, K. Uddin, J. Chevalier, Y. Guo, A. McGordon, P. Jennings, The effect of external compressive loads on the cycle lifetime of lithium-ion pouch cells, J Energy Storage. 13 (2017) 211–219. https://doi.org/10.1016/j.est.2017.07.021.

[19] Y. Zhao, Y. Patel, I.A. Hunt, K.M. Kareh, A.A. Holland, C. Korte, J.P. Dear, Y. Yue, G.J. Offer, Preventing lithium ion battery failure during high temperatures by externally applied compression, J Energy Storage. 13 (2017) 296–303. https://doi.org/10.1016/j.est.2017.08.001.

[20] X. Han, M. Ouyang, L. Lu, J. Li, Y. Zheng, Z. Li, A comparative study of commercial lithium ion battery cycle life in electrical vehicle: Aging mechanism identification, J Power Sources. 251 (2014) 38–54. https://doi.org/10.1016/j.jpowsour.2013.11.029.

[21] J.S. Edge, S. O'Kane, R. Prosser, N.D. Kirkaldy, A.N. Patel, A. Hales, A. Ghosh, W. Ai, J. Chen, J. Yang, S. Li, M.-C. Pang, L.B. Diaz, A. Tomaszewska, M.W. Marzook, K.N. Radhakrishnan,

H. Wang, Y. Patel, B. Wu, G.J. Offer, Lithium ion battery degradation: what you need to know, Phys Chem Chem Phys. 23 (2021) 8200–8221. https://doi.org/10.1039/d1cp00359c.

[22] C.R. Birkl, M.R. Roberts, E. McTurk, P.G. Bruce, D.A. Howey, Degradation diagnostics for lithium ion cells, J Power Sources. 341 (2017) 373–386. https://doi.org/10.1016/j.jpowsour.2016.12.011.

[23] R. Xiong, Y. Pan, W. Shen, H. Li, F. Sun, Lithium-ion battery aging mechanisms and diagnosis method for automotive applications: Recent advances and perspectives, Renew Sustain Energy Rev. 131 (2020) 110048. https://doi.org/10.1016/j.rser.2020.110048.

[24] N. Nitta, F. Wu, J.T. Lee, G. Yushin, Li-ion battery materials: present and future, Mater Today. 18 (2015) 252–264. https://doi.org/10.1016/j.mattod.2014.10.040.

[25] P. Arora, R.E. White, M. Doyle, Capacity Fade Mechanisms and Side Reactions in Lithium-Ion Batteries, J. Electrochem. Soc. 145 (1998) 3647. https://doi.org/10.1149/1.1838857.

[26] S.J. An, J. Li, C. Daniel, D. Mohanty, S. Nagpure, D.L. Wood, The state of understanding of the lithium-ion-battery graphite solid electrolyte interphase (SEI) and its relationship to formation cycling, Carbon. 105 (2016) 52–76. https://doi.org/10.1016/j.carbon.2016.04.008.

[27] R. Deshpande, M. Verbrugge, Y.-T. Cheng, J. Wang, P. Liu, Battery Cycle Life Prediction with Coupled Chemical Degradation and Fatigue Mechanics, J Electrochem Soc. 159 (2012) A1730–A1738. https://doi.org/10.1149/2.049210jes.

[28] M. Safari, M. Morcrette, A. Teyssot, C. Delacourt, Multimodal Physics-Based Aging Model for Life Prediction of Li-Ion Batteries, J Electrochem Soc. 156 (2009) A145. https://doi.org/10.1149/1.3043429.

[29] J.B. Goodenough, Y. Kim, Challenges for Rechargeable Li Batteries, Chem Mater. 22 (2010) 587–603. https://doi.org/10.1021/cm901452z.

[30] V.A. Agubra, J.W. Fergus, The formation and stability of the solid electrolyte interface on the graphite anode, J Power Sources. 268 (2014) 153–162. https://doi.org/10.1016/j.jpowsour.2014.06.024.

[31] X. Shen, Z. Tian, R. Fan, L. Shao, D. Zhang, G. Cao, L. Kou, Y. Bai, Research progress on silicon/carbon composite anode materials for lithium-ion battery, J Energy Chem. 27 (2017) 1067–1090. https://doi.org/10.1016/j.jechem.2017.12.012.

[32] R. Xiong, S. Ma, H. Li, F. Sun, J. Li, Toward a Safer Battery Management System: A Critical Review on Diagnosis and Prognosis of Battery Short Circuit, IScience. 23 (2020) 101010. https://doi.org/https://doi.org/10.1016/j.isci.2020.101010.

[33] C.Y. Ouyang, Z.Y. Zhong, M.S. Lei, Ab initio studies of structural and electronic properties of Li4Ti5O12 spinel, Electrochem Commun. 9 (2007) 1107–1112. https://doi.org/10.1016/j.elecom.2007.01.013.

[34] K. Edström, T. Gustafsson, J.O. Thomas, The cathode–electrolyte interface in the Li-ion battery, Electrochim Acta. 50 (2004) 397–403. https://doi.org/10.1016/j.electacta.2004.03.049.

[35] X. Li, Y. Xu, C. Wang, Suppression of Jahn–Teller distortion of spinel LiMn2O4 cathode, J Alloy Compd. 479 (2009) 310–313. https://doi.org/10.1016/j.jallcom.2008.12.081.

[36] K. Amine, J. Liu, I. Belharouak, S.-H. Kang, I. Bloom, D. Vissers, G. Henriksen, Advanced cathode materials for high-power applications, J Power Sources. 146 (2005) 111–115. https://doi.org/10.1016/j.jpowsour.2005.03.227.

[37] I. Belharouak, G.M. Koenig, K. Amine, Electrochemistry and safety of Li4Ti5O12 and graphite anodes paired with LiMn2O4 for hybrid electric vehicle Li-ion battery applications, J Power Sources. 196 (2011) 10344–10350. https://doi.org/10.1016/j.jpowsour.2011.08.079.

[38] W.-J. Zhang, Structure and performance of LiFePO4 cathode materials: A review, J Power Sources. 196 (2011) 2962–2970. https://doi.org/10.1016/j.jpowsour.2010.11.113.

[39] J.C. Burns, A. Kassam, N.N. Sinha, L.E. Downie, L. Solnickova, B.M. Way, J.R. Dahn, Predicting and Extending the Lifetime of Li-Ion Batteries, J Electrochem Soc. 160 (2013) A1451–A1456. https://doi.org/10.1149/2.060309jes.

[40] H.-J. Noh, S. Youn, C.S. Yoon, Y.-K. Sun, Comparison of the structural and electrochemical properties of layered Li[NixCoyMnz]O2 (x = 1/3, 0.5, 0.6, 0.7, 0.8 and 0.85) cathode material for lithium-ion batteries, J Power Sources. 233 (2013) 121–130. https://doi.org/10.1016/j.jpowsour.2013.01.063.

[41] C.M. Costa, Y.-H. Lee, J.-H. Kim, S.-Y. Lee, S. Lanceros-Méndez, Recent advances on separator membranes for lithium-ion battery applications: from porous membranes to solid electrolytes, Energy Storage Mater. 22 (2019) 346–375. https://doi.org/10.1016/j.ensm.2019.07.024.

[42] R. Yazami, Y.F. Reynier, Mechanism of self-discharge in graphite–lithium anode, Electrochim Acta. 47 (2002) 1217–1223. https://doi.org/10.1016/s0013-4686(01)00827-1.

[43] M. Kassem, C. Delacourt, Postmortem analysis of calendar-aged graphite/LiFePO4 cells, J Power Sources. 235 (2013) 159–171. https://doi.org/10.1016/j.jpowsour.2013.01.147.

[44] X.-G. Yang, Y. Leng, G. Zhang, S. Ge, C.-Y. Wang, Modeling of lithium plating induced aging of lithium-ion batteries: Transition from linear to nonlinear aging, J Power Sources. 360 (2017) 28–40. https://doi.org/10.1016/j.jpowsour.2017.05.110.

[45] X. Lin, J. Park, L. Liu, Y. Lee, A.M. Sastry, W. Lu, A Comprehensive Capacity Fade Model and Analysis for Li-Ion Batteries, J Electrochem Soc. 160 (2013) A1701–A1710. https://doi.org/10.1149/2.040310jes.

[46] T. Waldmann, M. Wilka, M. Kasper, M. Fleischhammer, M. Wohlfahrt-Mehrens, Temperature dependent ageing mechanisms in Lithium-ion batteries – A Post-Mortem study, J Power Sources. 262 (2014) 129–135. https://doi.org/10.1016/j.jpowsour.2014.03.112.

[47] M. Ouyang, D. Ren, L. Lu, J. Li, X. Feng, X. Han, G. Liu, Overcharge-induced capacity fading analysis for large format lithium-ion batteries with LiyNi1/3Co1/3Mn1/3O2+LiyMn2O4 composite cathode, J Power Sources. 279 (2015) 626–635. https://doi.org/10.1016/j.jpowsour.2015.01.051.

[48] R. Guo, L. Lu, M. Ouyang, X. Feng, Mechanism of the entire overdischarge process and overdischarge-induced internal short circuit in lithium-ion batteries, Sci Rep-Uk. 6 (2016) 30248. https://doi.org/10.1038/srep30248.

[49] G. Fan, K. Pan, M. Canova, J. Marcicki, X.G. Yang, Modeling of Li-Ion Cells for Fast Simulation of High C-Rate and Low Temperature Operations, J Electrochem Soc. 163 (2016) A666–A676. https://doi.org/10.1149/2.0761605jes.

[50] Y. Zheng, M. Ouyang, L. Lu, J. Li, Understanding aging mechanisms in lithium-ion battery packs: From cell capacity loss to pack capacity evolution, J Power Sources. 278 (2015) 287–295. https://doi.org/10.1016/j.jpowsour.2014.12.105.

[51] M. Ouyang, S. Gao, L. Lu, X. Feng, D. Ren, J. Li, Y. Zheng, P. Shen, Determination of the battery pack capacity considering the estimation error using a Capacity–Quantity diagram, Appl Energ. 177 (2016) 384–392. https://doi.org/10.1016/j.apenergy.2016.05.137.

[52] D. Liu, Z. Shadike, R. Lin, K. Qian, H. Li, K. Li, S. Wang, Q. Yu, M. Liu, S. Ganapathy, X. Qin, Q. Yang, M. Wagemaker, F. Kang, X. Yang, B. Li, Review of Recent Development of In Situ/Operando Characterization Techniques for Lithium Battery Research, Adv Mater. 31 (2019) 1806620. https://doi.org/10.1002/adma.201806620.

[53] C. Pastor-Fernández, M.-A. Gama-Valdez, W.D. Widanage, J. Marco, Gael.H. Chouchelamane, Identification and Quantification of Ageing Mechanisms in Lithium-ion Batteries Using the EIS Technique, 2016 Ieee Transp Electrification Conf Expo Itec. (2016) 1–6. https://doi.org/10.1109/itec.2016.7520198.

[54] D.E. Galvez-Aranda, A. Verma, K. Hankins, J.M. Seminario, P.P. Mukherjee, P.B. Balbuena, Chemical and mechanical degradation and mitigation strategies for Si anodes, J Power Sources. 419 (2019) 208–218. https://doi.org/10.1016/j.jpowsour.2019.02.054.

[55] M. Doyle, T.F. Fuller, J. Newman, Modeling of Galvanostatic Charge and Discharge of the Lithium/Polymer/Insertion Cell, J Electrochem Soc. 140 (1993) 1526-1533-1526–1533. https://doi.org/10.1149/1.2221597.

[56] T.F. Fuller, M. Doyle, J. Newman, Simulation and Optimization of the Dual Lithium Ion Insertion Cell, J Electrochem Soc. 141 (1994) 1-10-1–10. https://doi.org/10.1149/1.2054684.

[57] M. Dubarry, C. Truchot, B.Y. Liaw, Synthesize battery degradation modes via a diagnostic and prognostic model, J Power Sources. 219 (2012) 204–216. https://doi.org/10.1016/j.jpowsour.2012.07.016.

[58] G. Richardson, I. Korotkin, R. Ranom, M. Castle, J.M. Foster, Generalised single particle models for high-rate operation of graded lithium-ion electrodes: Systematic derivation and validation, Electrochim Acta. 339 (2020) 135862. https://doi.org/10.1016/j.electacta.2020.135862.

[59] J. Li, K. Adewuyi, N. Lotfi, R.G. Landers, J. Park, A single particle model with chemical/mechanical degradation physics for lithium ion battery State of Health (SOH) estimation, Appl Energ. 212 (2018) 1178–1190. https://doi.org/10.1016/j.apenergy.2018.01.011.

[60] J.M. Reniers, G. Mulder, D.A. Howey, Review and Performance Comparison of Mechanical-Chemical Degradation Models for Lithium-Ion Batteries, J Electrochem Soc. 166 (2019) A3189–A3200. https://doi.org/10.1149/2.0281914jes.